

Determination of the strong coupling constant using matched NNLO+NLLA predictions for hadronic event shapes in e^+e^- annihilations

G. Dissertori

*Institute for Particle Physics, ETH Zurich,
8093 Zurich, Switzerland
E-mail: dissertori@phys.ethz.ch*

A. Gehrmann–De Ridder

*Institute for Theoretical Physics, ETH Zurich,
8093 Zurich, Switzerland
E-mail: gehra@phys.ethz.ch*

T. Gehrmann

*Institut für Theoretische Physik, Universität Zürich, Winterthurerstrasse 190,
CH-8057 Zürich, Switzerland
E-mail: thomas.gehrmann@physik.unizh.ch*

E.W.N. Glover

*Institute for Particle Physics Phenomenology, Department of Physics,
University of Durham, Durham, DH1 3LE, UK
E-mail: e.w.n.glover@durham.ac.uk*

G. Heinrich

*Institute for Particle Physics Phenomenology, Department of Physics,
University of Durham, Durham, DH1 3LE, UK
E-mail: gudrun.heinrich@durham.ac.uk*

G. Luisoni

*Institut für Theoretische Physik, Universität Zürich, Winterthurerstrasse 190,
CH-8057 Zürich, Switzerland
E-mail: luisonig@physik.unizh.ch*

H. Stenzel

*II. Physikalisches Institut, Justus-Liebig Universität Giessen
Heinrich-Buff Ring 16, D-35392 Giessen, Germany
E-mail: Hasko.Stenzel@exp2.physik.uni-giessen.de*

ABSTRACT: We present a determination of the strong coupling constant from a fit of QCD predictions for six event-shape variables, calculated at next-to-next-to-leading order (NNLO) and matched to resummation in the next-to-leading-logarithmic approximation (NLLA). These event shapes have been measured in e^+e^- annihilations at LEP, where the data we use have been collected by the ALEPH detector at centre-of-mass energies between 91 and 206 GeV. Compared to purely fixed order NNLO fits, we observe that the central fit values are hardly affected, but the systematic uncertainty is larger because the NLLA part re-introduces relatively large uncertainties from scale variations. By combining the results for six event-shape variables and eight centre-of-mass energies, we find

$$\alpha_s(M_Z) = 0.1224 \pm 0.0009(\text{stat}) \pm 0.0009(\text{exp}) \pm 0.0012(\text{had}) \pm 0.0035(\text{theo}),$$

which improves previously published measurements at NLO+NLLA. We also carry out a detailed investigation of hadronisation corrections, using a large set of Monte Carlo generator predictions.

KEYWORDS: QCD, Jets, LEP Physics, NLO and NNLO Computations, resummation, strong coupling constant.

Contents

1. Introduction	1
2. Theoretical Framework	3
3. Determination of the strong coupling constant	7
4. Systematic Uncertainties of α_s	9
5. Combined Results	13
6. Systematic studies	15
6.1 $\ln R(\mu)$ -matching scheme	15
6.2 Normalisation and quark mass effects	16
6.3 Combination method	17
6.4 Hadronisation corrections from NLO+LL event generators	17
7. Discussion and Conclusions	21

1. Introduction

Event-shape distributions in e^+e^- annihilation have been measured with high accuracy at LEP at centre-of-mass energies between 91 and 206 GeV [1–5] and at the SLAC-SLD experiment at 91 GeV [6], as well as at the DESY PETRA collider at lower energies, e.g. by the JADE experiment [7]. Event-shape observables are infrared-safe variables designed to describe the structure of the hadronic final state. At leading order in perturbation theory, e^+e^- annihilation to hadrons occurs via $e^+e^- \rightarrow q\bar{q}$ and subsequent hadronisation to stable hadrons, resulting in a back-to-back (two-jet-like) structure of the event. At higher orders, gluon radiation off quarks will lead to deviations from this two-jet structure.

Fixed-order QCD corrections to event-shape distributions were calculated some time ago at next-to-leading order (NLO) [8–10], and more recently at next-to-next-to-leading order (NNLO) [11–16] for the six event-shape observables thrust T [17] (respectively $\tau = 1 - T$), heavy jet mass M_H [18], wide and total jet broadening B_W and B_T [19], C -parameter [20] and the two-to-three-jet transition parameter in the Durham algorithm, $-\ln y_3$ [21]. The definitions of these variables, which we denote collectively as y in the following, are summarised e.g. in [13, 22].

As the fixed order expansion is reliable only if the event-shape variable is sufficiently far away from its two-jet limit, i.e. away from $y \rightarrow 0$. This is because large logarithmic

corrections spoil the convergence of the perturbative expansion in the two-jet region, indicating the sensitivity to multiple soft gluon radiation. To obtain a reliable theoretical prediction in the full kinematical range, it is therefore necessary to resum these logarithms to all orders in perturbation theory and to match the resummed result to the fixed order calculation.

Until very recently, the theoretical state-of-the-art description of event-shape distributions over the full kinematic range was based on the matching of the next-to-leading-logarithmic approximation (NLLA) [23] onto the fixed next-to-leading order [8–10] calculation. Now that the NNLO results are available, the matching of the resummed result in the next-to-leading-logarithmic approximation onto the NNLO calculation has been performed [24] for all six event shapes mentioned above in the so-called $\ln R$ -matching scheme [23]. It was found that the difference between NLLA+NNLO and NNLO is largely restricted to the two-jet region, while NLLA+NLO differed from pure NLO in normalisation throughout the full kinematical range. For the thrust distribution, logarithmic corrections reaching beyond the NLL approximation have been calculated recently [25] using Soft-Collinear Effective Theory (SCET) [26].

In the theoretical description of event-shape observables within perturbative QCD, the only free parameter is the strong coupling constant α_s , such that a fit of QCD predictions to the data for these observables lends itself to determine the strong coupling constant with high precision. Several determinations of α_s based on NNLO results have been performed recently: using NNLO predictions [13] for the six event shapes listed above, a determination of α_s based on ALEPH data [1] has been performed [27], where the systematic uncertainty from renormalisation scale variations was found to be reduced by a factor of two as compared to the fit based on NLO predictions only. After the NNLO+NLLA calculations for the six event shapes have become available [24], a determination of α_s based on JADE data has been carried out in [28].

Further, there are several studies based on thrust only: Using ALEPH and OPAL data for the thrust distribution and combining the theoretical NNLO prediction with infrared logarithms resummed within the SCET formalism, a precise determination of α_s has also been performed in [25]. A re-evaluation of the non-perturbative contribution to the thrust distribution is presented in [29], where the NNLO results of [11, 13] have been matched to resummation at NLL accuracy and then used for a combined determination of both the low-scale effective coupling α_0 and $\alpha_s(M_Z)$.

A very recent study of non-perturbative corrections based on moments of event shapes has been carried out in [30, 31], ref. [31] containing also a determination of both α_0 and $\alpha_s(M_Z)$. However, these studies are based on NLO calculations only. NNLO predictions for event shape moments can be found in [32].

The agreement in the two-jet region of the matched prediction with hadron-level data is still far from being perfect, the discrepancy being attributed mainly to non-perturbative hadronisation corrections, but also to missing subleading logarithms, electroweak corrections and quark mass effects. In fact, based on the results of [25], one can estimate that the subleading logarithms can account for roughly half of the discrepancy between the parton-level matched NLLA+NNLO prediction and the hadron level data.

While significant progress has been made for the perturbative calculations, the non-perturbative corrections for hadronisation needed to extract the value of α_s from event-shape distributions are still obtained from Monte Carlo event generators based on leading-logarithmic (LL) parton showers and fragmentation models [1,27]. The hadronisation itself is presently parametrised by string- or cluster fragmentation models but the simulation of the multi-parton final state can now be performed at NLO+LL, which is in principle more consistent with the NNLO+NLLA calculation we use in our fits. We therefore investigate the performance of this type of generators taking HERWIG++ [33] as reference, which represents a modern event generator allowing optionally the inclusion of NLO calculations according to different schemes.

In this paper, we present a determination of the strong coupling constant based on matched NLLA+NNLO results for six event-shape variables. Hadronisation corrections and quark mass effects (at least to NLO [34]) have been included in the procedure. We first review the theoretical framework in section 2 before proceeding to the comparison with data in section 3. The method used for the fit follows closely that described in [1,27], but some improvements to the method used in [1] have been made which will be explained in section 3. Systematic uncertainties for individual determinations of $\alpha_s(Q)$ from different variables at different energies are presented in section 4. Combined results are given in section 5 and further systematic studies concerning the hadronisation corrections, the scheme of matching NLLA to NNLO, the normalisation and quark mass correction procedure as well as the combination method are discussed in section 6. Finally our findings are summarized in section 7.

2. Theoretical Framework

The fixed-order QCD description of the experimentally measured event-shape distributions

$$\frac{1}{\sigma_{\text{had}}} \frac{d\sigma}{dy}$$

starts from the perturbative expansion

$$\frac{1}{\sigma_0} \frac{d\sigma}{dy}(y, Q, \mu) = \bar{\alpha}_s(\mu) \frac{dA}{dy}(y) + \bar{\alpha}_s^2(\mu) \frac{dB}{dy}(y, x_\mu) + \bar{\alpha}_s^3(\mu) \frac{dC}{dy}(y, x_\mu) + \mathcal{O}(\bar{\alpha}_s^4), \quad (2.1)$$

where

$$\bar{\alpha}_s = \frac{\alpha_s}{2\pi}, \quad x_\mu = \frac{\mu}{Q},$$

and where A , B and C are the perturbatively calculated coefficients [13] at LO, NLO and NNLO. They have been computed with the parton-level event generator program **EERAD3**, which contains the relevant matrix elements with up to five external partons [35–38], combined using an infrared antenna subtraction method [39]. A recently discovered inconsistency in the treatment of large-angle soft radiation [14] in the original **EERAD3** implementation has been corrected, resulting in numerically minor changes to the NNLO coefficient in the kinematical region relevant to the phenomenological studies here. In the deep two-jet region, e.g. $(1 - T) \ll 0.02$, these soft correction terms turn out to be

numerically significant. They account for an initially observed discrepancy between the EERAD3 results and the logarithmic contributions (computed within SCET) to the thrust distribution to NNLO [25], which are now in full agreement.

All coefficients are normalised to the tree-level cross section for $e^+e^- \rightarrow q\bar{q}$, σ_0 . For massless quarks, this normalisation cancels all electroweak coupling factors, and the dependence of (2.1) on the collision energy is only through α_s and x_μ . Summation over massless quark flavours in σ_0 and $d\sigma/dy$ results in a constant normalisation factor which cancels exactly in the ratio of these quantities.

Predictions for the experimentally measured event-shape distributions are then obtained by normalising to σ_{had} as

$$\frac{1}{\sigma_{\text{had}}} \frac{d\sigma}{dy}(y, Q, \mu) = \frac{\sigma_0}{\sigma_{\text{had}}(Q, \mu)} \frac{1}{\sigma_0} \frac{d\sigma}{dy}(y, Q, \mu). \quad (2.2)$$

For massless quarks, all electroweak coupling factors cancel in $\sigma_0/\sigma_{\text{had}}$.

In all expressions, the scale dependence of α_s is determined according to the three-loop running:

$$\alpha_s(\mu^2) = \frac{2\pi}{\beta_0 L} \left(1 - \frac{\beta_1}{\beta_0^2} \frac{\ln L}{L} + \frac{1}{\beta_0^2 L^2} \left(\frac{\beta_1^2}{\beta_0^2} (\ln^2 L - \ln L - 1) + \frac{\beta_2}{\beta_0} \right) \right), \quad (2.3)$$

where $L = 2 \ln(\mu/\Lambda_{\overline{\text{MS}}}^{(N_F)})$ and β_i are the $\overline{\text{MS}}$ -scheme coefficients listed in [13].

The assumption of vanishing quark masses, which was used in all expressions for differential distributions up to here, is only partly justified, especially for the LEP1 data, where bottom quark mass corrections can be relevant at the per cent level [40]. The effect scales with M_b^2/Q^2 and decreases to 0.2-0.3% at 200 GeV. We take into account bottom mass effects by retaining the massless $N_F = 5$ expressions derived above and adding the difference between the massless and massive LO and NLO coefficients A and B [34],

$$\frac{1}{\sigma_{\text{had}}} \frac{d\sigma}{dy}(y, Q, \mu) = \frac{1}{\sigma_{\text{had}}} \left((1 - r_b(Q)) \frac{d\sigma}{dy}_{\text{massless}} + r_b(Q) \frac{d\sigma}{dy}_{\text{massive}} \right). \quad (2.4)$$

A pole b-quark mass $M_b = 4.5 \text{ GeV}/c^2$ was used and Standard Model values were taken for the fraction $r_b(Q)$ of $b\bar{b}$ events. In this case, the electroweak coupling factors no longer cancel in the ratio $\sigma_0/\sigma_{\text{had}}$, and the summation over quark flavours has to be carried out explicitly.

For σ_{had} an NNLO calculation ($\mathcal{O}(\alpha_s^2)$ in QCD) [41] including mass corrections for the b-quark up to $\mathcal{O}(\alpha_s)$, and including the leading mass terms to $\mathcal{O}(\alpha_s^2)$, was used to calculate the correction $\sigma_0/\sigma_{\text{had}}$. A genuine $\mathcal{O}(\alpha_s^3)$ -expression for (2.2) can be obtained by expanding the ratio $\sigma_0/\sigma_{\text{had}}$, as done in [13].

Next-to-leading order electroweak corrections to event shape distributions in e^+e^- annihilation were computed very recently [42]. Using the event selection cuts and event shape definitions as applied in the experimental analysis [1], one observes substantial electroweak corrections to σ_{had} and $d\sigma/dy$. These corrections cancel to a very large extent in the ratio (2.2). In the kinematical range used in the α_s determination below, the total electroweak corrections are at the level of two per cent at LEP1 and at most five per cent at LEP2.

Genuine weak corrections from virtual massive gauge boson loops or fermion loops amount to one per mille or less at both LEP1 and LEP2. The corrections are thus much lower than initially anticipated from partial calculations of higher-order electroweak contributions [43]. Since the experimental data were corrected for photon radiation effects using PYTHIA, it is not straightforward to include the electroweak corrections, and requires further study.

The resummation of large logarithmic corrections in the $y \rightarrow 0$ limit starts from the integrated cross section:

$$R(y, Q, \mu) \equiv \frac{1}{\sigma_{\text{had}}} \int_0^y \frac{d\sigma(x, Q, \mu)}{dx} dx, \quad (2.5)$$

which has the following fixed-order expansion:

$$R(y, Q, \mu) = 1 + \mathcal{A}(y) \bar{\alpha}_s(\mu) + \mathcal{B}(y, x_\mu) \bar{\alpha}_s^2(\mu) + \mathcal{C}(y, x_\mu) \bar{\alpha}_s^3(\mu) + \mathcal{O}(\bar{\alpha}_s^4). \quad (2.6)$$

The fixed-order coefficients \mathcal{A} , \mathcal{B} , \mathcal{C} can be obtained by integrating the distribution (2.1) normalised to σ_{had} (2.2) and using $R(y_{\text{max}}, Q, \mu) = 1$ to all orders, where y_{max} is the maximum kinematically allowed value for the event-shape variable y .

In the limit $y \rightarrow 0$ one observes that the perturbative α_s^n -contribution to $R(y)$ diverges like $\alpha_s^n L^{2n}$, with $L = -\ln y$ ($L = -\ln(y/6)$ for $y = C$). This leading logarithmic (LL) behaviour is due to multiple soft gluon emission at higher orders, and the LL coefficients exponentiate, such that

$$\ln R(y) \sim L g_1(\alpha_s L),$$

where $g_1(\alpha_s L)$ is a power series in its argument.

For the event-shape observables considered here, and assuming massless quarks, leading and next-to-leading logarithmic (NLL) corrections can be resummed to all orders in the coupling constant, such that

$$R(y, Q, \mu) = (1 + C_1 \bar{\alpha}_s) e^{(L g_1(\alpha_s L) + g_2(\alpha_s L))}, \quad (2.7)$$

where terms beyond NLL have been consistently omitted, and $\mu = Q$ ($x_\mu = 1$) is used. By differentiating expression (2.7) with respect to y , one recovers the resummed differential event-shape distributions, which yield an accurate description for $y \rightarrow 0$.

Closed analytic forms for the LL and NLL resummation functions $g_1(\alpha_s L)$, $g_2(\alpha_s L)$ are available for τ [44], M_H [45], B_W and B_T [46, 47], C [48] and y_3 [49]. They can be expanded as a power series, such that

$$\ln R(y, Q, \mu) = \sum_{i=1}^{\infty} \sum_{n=1}^{i+1} G_{i, i+2-n} \bar{\alpha}_s^i L^{i+2-n}. \quad (2.8)$$

In order to obtain a reliable description of the event-shape distributions over a wide range in y , it is mandatory to combine fixed order and resummed predictions. However, in order to avoid the double counting of terms common to both, the two predictions have to be matched onto each other. A number of different matching procedures have been proposed in the literature and for a review we refer the reader to Ref. [22]. The most commonly

used procedure is the so-called $\ln R$ -matching [23]. In this particular scheme, all matching coefficients can be extracted analytically from the resummed calculation, while most other schemes require the numerical extraction of some of the matching coefficients from the distributions at fixed order. Since the fixed order calculations face numerical instabilities in the region $y \rightarrow 0$, the numerical extraction of matching coefficients is prone to large errors. Therefore we restrict ourselves to the $\ln R$ -matching, studying two different variants of the latter for the present analysis. In the $\ln R$ -matching scheme, the NLLA+NNLO expression is

$$\begin{aligned} \ln(R(y, \alpha_s)) &= L g_1(\alpha_s L) + g_2(\alpha_s L) \\ &+ \bar{\alpha}_s \left(\mathcal{A}(y) - G_{11}L - G_{12}L^2 \right) + \\ &+ \bar{\alpha}_s^2 \left(\mathcal{B}(y) - \frac{1}{2}\mathcal{A}^2(y) - G_{22}L^2 - G_{23}L^3 \right) \\ &+ \bar{\alpha}_s^3 \left(\mathcal{C}(y) - \mathcal{A}(y)\mathcal{B}(y) + \frac{1}{3}\mathcal{A}^3(y) - G_{33}L^3 - G_{34}L^4 \right) + \mathcal{O}(\bar{\alpha}_s^4). \end{aligned} \quad (2.9)$$

The matching coefficients appearing in this expression can be obtained from (2.8) and are given in [24], where we refer the reader to for more details. Quark mass corrections to this expression are included by retaining the mass dependence of the fixed-order coefficients \mathcal{A} and \mathcal{B} , which follow from the mass-corrected coefficient functions (2.4) and the mass-dependent total hadronic cross section.

The coefficients in (2.9) explicitly depend on x_μ , thereby stabilising the scale dependence of the theoretical prediction:

$$\alpha_s \rightarrow \alpha_s(\mu), \quad (2.10)$$

$$\begin{aligned} \mathcal{B}(y) &\rightarrow \mathcal{B}(y, \mu) = \beta_0 \ln x_\mu \mathcal{A}(y) + \mathcal{B}(y), \\ \mathcal{C}(y) &\rightarrow \mathcal{C}(y, \mu) = (\beta_0 \ln x_\mu)^2 \mathcal{A}(y) + \ln x_\mu [2\beta_0 \mathcal{B}(y) + \beta_1 \mathcal{A}(y)] + \mathcal{C}(y), \end{aligned} \quad (2.11)$$

$$g_2(\alpha_s L) \rightarrow g_2(\alpha_s L, \mu^2) = g_2(\alpha_s L) + \frac{\beta_0}{2\pi} (\alpha_s L)^2 g_1'(\alpha_s L) \ln x_\mu, \quad (2.12)$$

$$\begin{aligned} G_{22} &\rightarrow G_{22}(\mu) = G_{22} + \beta_0 G_{12} \ln x_\mu, \\ G_{33} &\rightarrow G_{33}(\mu) = G_{33} + 2\beta_0 G_{23} \ln x_\mu, \end{aligned} \quad (2.13)$$

where g_1' denotes the derivative of g_1 with respect to its argument. This scale variation also exemplifies a tension between NLLA and NNLO, since the NNLO coefficients compensate the renormalisation scale variation of α_s up to two loops, while the NLLA coefficients only compensate the one-loop variation. A fully consistent matching, including the full scale dependence, is therefore only accomplished by combining NLLA+NLO or NNLLA+NNLO. In order to assess the effect of this incomplete compensation of scale-dependent terms, we have computed the two-loop terms proportional to x_μ in the above resummation and

matching functions, i.e. the scale-dependent logarithms appearing in g_3 and in the associated matching coefficients G_{21} and G_{32} , and recomputed the theoretical error in this new matching scheme, which we call the $\ln R(\mu)$ -scheme. In this scheme the NLLA+NNLO expression becomes

$$\begin{aligned} \ln(R(y, \alpha_S)) &= L g_1(\alpha_S L) + g_2(\alpha_S L) + \bar{\alpha}_S g_3(\alpha_S L) \\ &+ \bar{\alpha}_S (\mathcal{A}(y) - G_{11}L - G_{12}L^2) + \\ &+ \bar{\alpha}_S^2 \left(\mathcal{B}(y) - \frac{1}{2} \mathcal{A}^2(y) - G_{21}L - G_{22}L^2 - G_{23}L^3 \right) \\ &+ \bar{\alpha}_S^3 \left(\mathcal{C}(y) - \mathcal{A}(y)\mathcal{B}(y) + \frac{1}{3} \mathcal{A}^3(y) - G_{32}L^2 - G_{33}L^3 - G_{34}L^4 \right) + \mathcal{O}(\bar{\alpha}_S^4), \end{aligned} \quad (2.14)$$

where the μ -dependence of g_3 is

$$\begin{aligned} g_3(\alpha_S L) \rightarrow g_3(\alpha_S L, \mu^2) &= g_3(\alpha_S L) + (\alpha_S L) \ln x_\mu \left[\beta_0 g_2'(\alpha_S L) + \frac{\beta_1}{2\pi} (\alpha_S L) g_1'(\alpha_S L) \right] \\ &+ \frac{\beta_0^2}{\pi} (\alpha_S L)^2 (\ln x_\mu)^2 \frac{d}{d(\alpha_S L)} \left(\frac{d}{dL} (L g_1(\alpha_S L)) \right). \end{aligned} \quad (2.15)$$

The "bare" $g_3(\alpha_S L)$ is not known and is put to zero, whereas the renormalisation scale dependence is proportional to the derivatives of g_1 and g_2 . In order to have a correct compensation of the renormalisation scale dependence the following further substitutions are made

$$\begin{aligned} G_{21} &\rightarrow G_{21}(\mu^2) = G_{21} + \beta_0 G_{11} \ln x_\mu, \\ G_{32} &\rightarrow G_{32}(\mu^2) = G_{32} + (\beta_0 \ln x_\mu)^2 G_{12} + \ln x_\mu (2\beta_0 G_{22} + 2\beta_1 G_{12}). \end{aligned} \quad (2.16)$$

As discussed in detail in Section 6 below, the resulting theoretical error is considerably lower than in the standard $\ln R$ -matching scheme, and comparable to the error obtained in [25], where the thrust distribution was computed beyond NLLA and matched to NNLO [11, 13].

In order to ensure the vanishing of the matched expression at the kinematical boundary y_{\max} , the further substitution [22] is made:

$$L \longrightarrow \tilde{L} = \frac{1}{p} \ln \left(\left(\frac{y_0}{x_L y} \right)^p - \left(\frac{y_0}{x_L y_{\max}} \right)^p + 1 \right), \quad (2.17)$$

where $y_0 = 6$ for $y = C$ and $y_0 = 1$ otherwise. The values $p = 1$ and $x_L = 1$ are taken as default. The arbitrariness in the choice of the logarithm to be resummed can be quantified by varying the constant x_L .

3. Determination of the strong coupling constant

As in the analysis of Ref. [27] we have studied the six event-shape distributions thrust T [17], heavy jet mass M_H [18], total and wide jet broadening (B_T, B_W) [19], C-parameter

C [20] and the two-to-three-jet transition parameter in the Durham algorithm $-\ln y_3$ [21]. The definitions of these variables and a discussion of their properties can be found in Refs. [1] and [22, 50].

The measurements have been carried out by the ALEPH collaboration [1]¹, at centre-of-mass energies of 91.2, 133, 161, 172, 183, 189, 200 and 206 GeV. Earlier measurements and complementary data sets from the LEP experiments and from SLD can be found in Refs. [2–6]. The event-shape distributions were computed using the reconstructed momenta and energies of charged and neutral particles. The measurements have been corrected for detector effects, i.e. the final distributions correspond to the so-called particle (or hadron) level. The particle level is defined by stable hadrons with a lifetime longer than 10^{-9} s after hadronisation and leptons according to the definition given in [51]. In addition, at LEP2 energies above the Z peak they were corrected for initial-state radiation effects. At energies above 133 GeV, backgrounds from 4-fermion processes, mainly from W-pair production and also ZZ and $Z\gamma^*$, were subtracted following the procedure given in [1]. The experimental uncertainties were estimated by varying event and particle selection cuts. They are below 1% at LEP1 and slightly larger at LEP2. For further details we refer to Ref. [1].

The determination of the coupling constant from these data follows very closely the approach chosen in Refs. [1, 27]. The perturbative predictions for the distributions, as described in section 2, are calculated to the same order of perturbation theory for all of these variables and fit to the data. The measurements from several variables are combined, since this yields a better estimator of α_s than using a single variable. Furthermore, the spread of values of α_s is an independent estimate of the theoretical uncertainty. At centre-of-mass energies above the Z peak the statistical uncertainties are larger and background conditions are more difficult than at the peak. Therefore a combination of measurements is particularly important for those energies. We apply the same combination procedure as described in [1, 27], which is based on weighted averages and takes into account correlations between the event-shape variables. However, in this paper we also investigate a combination procedure which excludes the perturbative uncertainty as weight, in order to evaluate the stability of our nominal combination method. Note that for energies above M_Z we adopt the same treatment of statistical uncertainties as in [1, 27]. The same holds for the fit ranges chosen at the LEP2 energies [27], whereas for the LEP1 data the fit ranges have been slightly extended, motivated by the expected better description of the two-jet range by the resummed calculations.

In this paper we present fits of matched NNLO+NLLA predictions and compare them to pure NNLO and matched NLO+NLLA calculations as used in the analyses of Refs. [1, 27]. The nominal value for the renormalisation scale $x_\mu = \mu/Q$ is unity. The perturbative QCD prediction is corrected for hadronisation and resonance decays by means of a transition matrix, which is computed with the Monte Carlo generators PYTHIA [52], HERWIG [53] and ARIADNE [54], all tuned to global hadronic observables at M_Z [51]. The parton level is defined by the quarks and gluons present at the end of the parton shower in PYTHIA and HERWIG and the partons resulting from the colour dipole radiation in ARIADNE.

¹The tables with numbers and uncertainties for all variables can be found at <http://aleph.web.cern.ch/aleph/QCD/alephqcd.html>.

Corrected measurements of event-shape distributions are compared to the theoretical calculation at particle level. In section 6 we investigate the use of the NLO+LL event generator HERWIG++.

The value of α_s is determined at each energy using a binned least-squares fit. The fit programs of Ref. [27] have been extended to incorporate the NNLO+NLLA calculations. Only statistical uncertainties arising from the limited number of observed events, from the number of simulated events used to calculate hadronisation and detector corrections and from the integration procedure of the NNLO coefficient functions are included in the χ^2 of the fit. Its quality is good for all variables at all energies. Nominal results for thrust and $-\ln y_3$, based on (2.9) and using the fitted values of α_s , are shown in Fig. 1, together with the measured distributions. The resulting measurements of $\alpha_s(Q)$ for all six event shapes are given in Table 1 for 91.2 to 172 GeV and in Table 2 for 183 to 206 GeV. Comparisons of fits using different perturbative approximations are shown in Fig. 2 for the variables thrust and y_3 and results for all variables at LEP1 are given in Table 3.

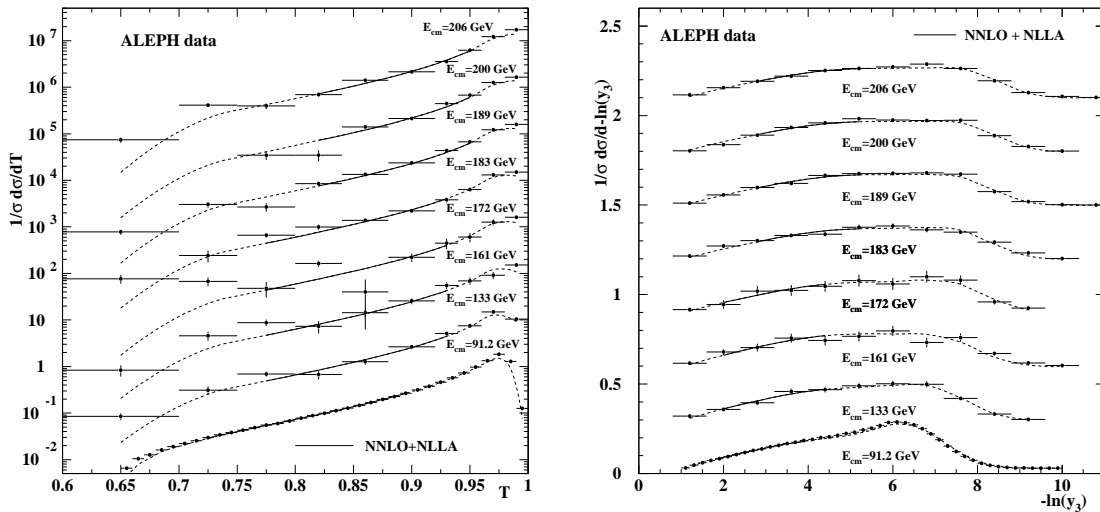


Figure 1: Distributions measured by ALEPH, after correction for backgrounds and detector effects, of thrust and the two-to-three-jet transition parameter in the Durham algorithm at energies between 91.2 and 206 GeV, together with the fitted NNLO+NLLA QCD predictions. The error bars correspond to the statistical uncertainties. The fit ranges cover the central regions indicated by the solid curves, the theoretical predictions extrapolate well outside these fit ranges, as shown by the dotted curves. The plotted distributions are scaled by arbitrary factors for presentation.

4. Systematic Uncertainties of α_s

For a description of the determination and treatment of experimental systematic uncertainty we refer to Refs. [1, 27], since the identical approach is taken for this analysis. Similarly, the analysis of theoretical uncertainties goes along the lines of these earlier pub-

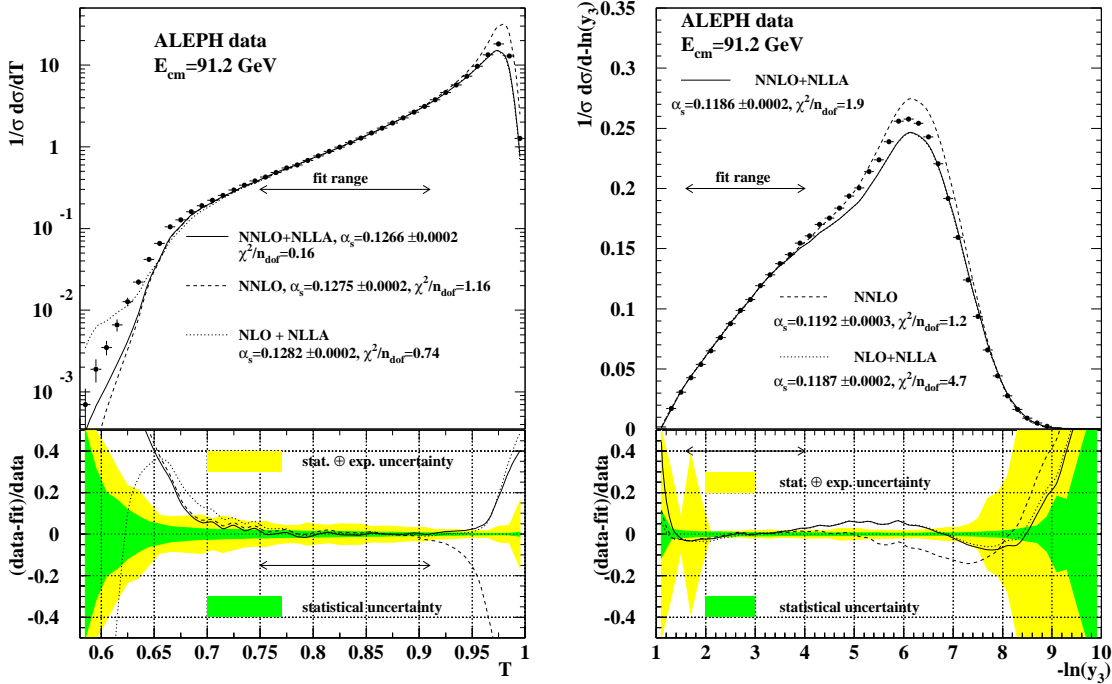


Figure 2: Distributions measured by ALEPH at LEP1, after correction for detector effects, of thrust and the two-to-three-jet transition parameter in the Durham algorithm. Fitted QCD predictions at different orders of perturbation theory are overlaid. The lower insets show a relative comparison of data and QCD fits.

lications. The main source of arbitrariness in the predictions is the choice of the renormalisation scale x_μ and of the logarithmic rescaling variable x_L . The residual dependence of the fitted value of $\alpha_s(M_Z)$ on the renormalisation scale is shown in Fig. 3, for the same two variables as in the previous figures. Most notably, the matching of NLLA terms to the NNLO prediction does not lead to a reduced scale dependence, compared to pure NNLO only, but at least to an improvement compared to NLO+NLLA. This could be anticipated by the discussion in section 2 on the scale dependence of the NNLO and NLLA predictions. A further study of this particular aspect is described in section 6 below.

The systematic uncertainty related to missing higher orders is estimated with the uncertainty-band method recommended in Ref. [22]. Briefly, this method derives the uncertainty of α_s from the uncertainty of the theoretical prediction for the event-shape distribution and proceeds in three steps. First a reference perturbative prediction, here NNLO+NLLA with $x_\mu = 1$ and $x_L = 1$, is determined using the value of α_s obtained from the combination of the six variables and eight energies, as explained in section 5. Then variants of the prediction with different choices for x_μ and x_L , for the kinematic constraint y_{\max} and the modification degree power p are calculated with the same value of α_s . A variation of the matching scheme as advocated in Ref. [22] was not included in the list of variants, since no R -matching scheme is presently available at NNLO+NLLA. In each

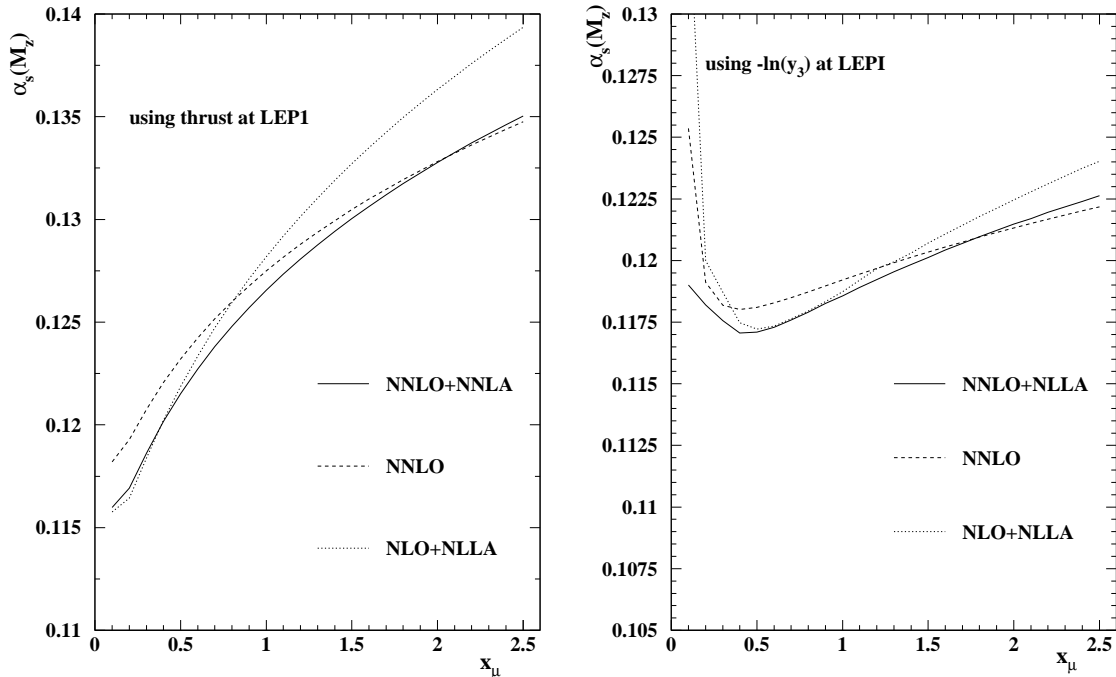


Figure 3: Dependence of the extracted α_s -value on the renormalisation scale when fitting the distributions of thrust (left) and the two-to-three-jet transition parameter in the Durham algorithm (right) with predictions at NNLO+NLLA (solid), NNLO (dashed) and NLO+NLLA (dotted).

bin of the distribution for a given variable, the largest upward and downward differences with respect to the reference prediction are taken to define an uncertainty band around the reference theory. In the last step, the value of α_s in the reference prediction is varied, in order to find the range of values which result in predictions lying inside the uncertainty band for the fit range under consideration. In contrast to the original method [22] we do not require the reference prediction to lie strictly inside the uncertainty band, since for the present NNLO+NLLA calculations the latter is still subject to statistical fluctuations. Instead, we make a fit of the reference theory with α_s as free parameter to the uncertainty band, which includes the statistical uncertainty on the C coefficient, as in Ref. [27]. The values of α_s fitted to the upper and lower contour of the uncertainty band finally set the perturbative systematic uncertainty. The upward and downward uncertainties are very similar in magnitude and the larger is quoted as symmetric uncertainty. The method is illustrated in Fig. 4 for thrust and the two-to-three-jet transition parameter in the Durham algorithm $-\ln y_3$.

The combined value of α_s , used to derive the systematic perturbative error, depends itself on the theoretical error. Hence the procedure of calculating the α_s combination and its perturbative error is iterated until convergence is reached, typically after two iterations.

At LEP2 energies the statistical fluctuations are large. In order to avoid biases from

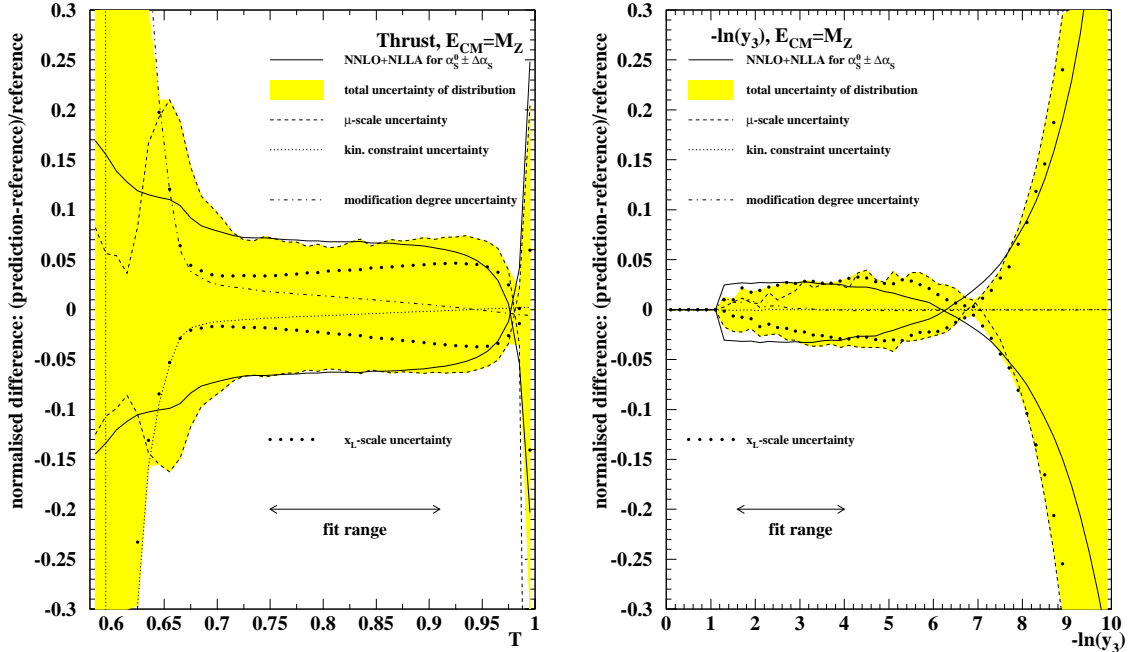


Figure 4: Theoretical uncertainties for the distributions of thrust (left) and the two-to-three-jet transition parameter in the Durham algorithm (right) at LEP1. The filled area represents the perturbative uncertainties of the distribution for a given value α_s^0 . The curves show the reference prediction with $\alpha_s^0 \pm \Delta\alpha_s$. The theoretical uncertainty $\Delta\alpha_s$ is derived from a fit of the reference theory to the contour of the uncertainty band for the actual fit range.

downward fluctuations, the theoretical uncertainties are calculated with the value of α_s obtained by the global combination procedure. For each energy point and in each variable, the combined α_s is evolved to the appropriate energy scale and the uncertainty is calculated for the fit range used for the different variables.

An additional error is evaluated for the b-quark mass correction procedure. This correction has only been calculated to $\mathcal{O}(\alpha_s^2)$ for the differential coefficients; no resummed and NNLO expressions are yet available. We have updated the calculations for the massive coefficients used in [1, 27] to include now three different sets for $M_b = 4.0, 4.5$ and 5.0 GeV/c^2 . The difference in α_s obtained with these different sets is taken as systematic error. The difference between the massless and massive expression for the hadronic cross section is already rather small and not included in this estimate.

The total perturbative uncertainty quoted in the tables is the quadratic sum of the errors for missing higher orders and for the mass correction procedure. The total perturbative error is between 3% and 5% at M_Z and decreases to between 2% and 3% at LEP2 energies.

The hadronisation model uncertainty is estimated by comparing the standard hadron-level event generator programs HERWIG and ARIADNE to PYTHIA for both hadroni-

sation and detector corrections. The same set of corrections as in Ref. [1] is used. Both corrections are calculated with the same generator in order to obtain a coherent description at the hadron level. The maximum change with respect to the nominal result using PYTHIA is taken as the systematic error. At LEP2 energies the hadronisation model uncertainty is again subject to statistical fluctuations. These fluctuations are observed from one energy to the next and originate from limited statistics of the fully simulated detector-correction functions. Since non-perturbative effects are expected to decrease with $1/Q$, the energy evolution of hadronisation errors has been fitted to a simple $A + B/Q$ parametrisation. The fit was performed for each variable separately. In the fit procedure a weight scaling with luminosity is assigned to the hadronisation uncertainty at each energy point. This ensures that the hadronisation uncertainty at M_Z , which is basically free of statistical fluctuations, is not altered by the procedure. As in the case of experimental systematic uncertainties, the hadronisation uncertainty is essentially identical to that published in [1]. In section 6 we present an attempt to use modern event generators to estimate the hadronisation corrections.

The perturbative component of the error, which is the dominant source of uncertainty in most cases, is highly correlated between the energy points. The perturbative errors decrease with increasing Q , and faster than the coupling constant itself. The overall error is in general dominated by the renormalisation scale dependence.

5. Combined Results

The measurements obtained from the six different variables using NNLO+NLLA calculations are combined into a single measurement per energy using weighted averages. The same procedure as in Refs. [1, 27] is applied here. However, we investigate also the impact of the theoretical uncertainties in the calculations of the weights, as described in section 6 below.

In Table 7 the weighted averages are given for all LEP1 and LEP2 data, as well as for the LEP2 data only. Essentially identical results with very similar errors are found. The fitted values of α_s at the various centre-of mass energies are displayed in Fig. 5 and compared to the QCD three-loop formula for the running of the coupling constant. Excellent agreement of the data with the expected energy dependence is observed.

In Table 8 we compare the combined results obtained at NNLO+NLLA accuracy to the results at NNLO and NLO+NLLA. The numbers given in Table 8 supersede those published in [27] at NNLO and NLO+NLLA and can be traced back to the following changes in the present analysis

- for the normalisation to σ_{had} an expansion of the ratio $\sigma_0/\sigma_{\text{had}}$ was applied in Refs. [1, 27], while here the exact value is used;
- new massive coefficients using $M_b = 4.5 \text{ GeV}/c^2$ up to NLO are used;
- a massive expression for σ_{had} is now adopted;

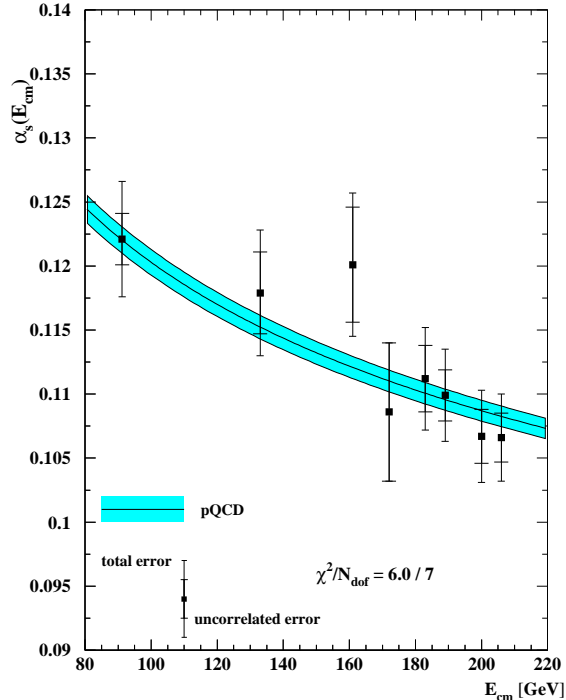


Figure 5: The measurements of the strong coupling constant α_s between 91.2 and 206 GeV. The results using the six different event-shape variables are combined with correlations taken into account. The inner error bars exclude the perturbative uncertainty, which is expected to be highly correlated between the measurements. The outer error bars indicate the total error. A fit of the three-loop evolution formula using the uncorrelated errors is shown. The shaded area corresponds to the uncertainty in the fit parameter $\Lambda_{\overline{\text{MS}}}^{(5)} = 284 \pm 14$ MeV of the three-loop formula, eq. (2.3).

- for a given observable and energy, the same fit ranges (given in Tables 1 and 2) are applied to different theoretical predictions;
- a small transcription error in the fit program used in [27] when calculating the NNLO term for $-\ln y_3$ is corrected;
- the previously incomplete treatment of large-angle soft radiation [14] in EERAD3 is corrected, resulting in minor numerical shifts in the NNLO coefficients;
- while in [1, 27] the NLO+NLLA predictions were obtained by a numerical derivative of R (cf. eq. (2.5)), we now compute the differential distributions analytically for the resummed part, which yields a better numerical stability. We apply this procedure also to NNLO+NLLA.

As was anticipated in section 2, the matching of the NNLO prediction with the resummation at NLLA introduces a renormalisation scale dependence which is absent in the pure NNLO case, as described in detail in section 2. This is reflected by the increased

perturbative and finally total uncertainty of the NNLO+NLLA result compared to NNLO, as can be seen by comparing Table 5 for the combined value of $\alpha_s(M_Z)$ at different energies at NNLO+NLLA with Table 6 at NNLO. However, compared to the NLO+NLLA fit, an improvement of more than 20% is obtained for the perturbative error. The central values of the fits for the different approximations turn out to be pretty similar. The fitted values of the coupling constant as found from the various event-shape variables, combined over all energies, are shown in Fig. 6. Besides the larger uncertainties, at NNLO+NLLA we observe the same reduced scatter of the results compared to NLO+NLLA as already reported previously [27]. However, the effect is not as strong as going from a NLO fit (where the scatter is largest) to a pure NNLO fit.

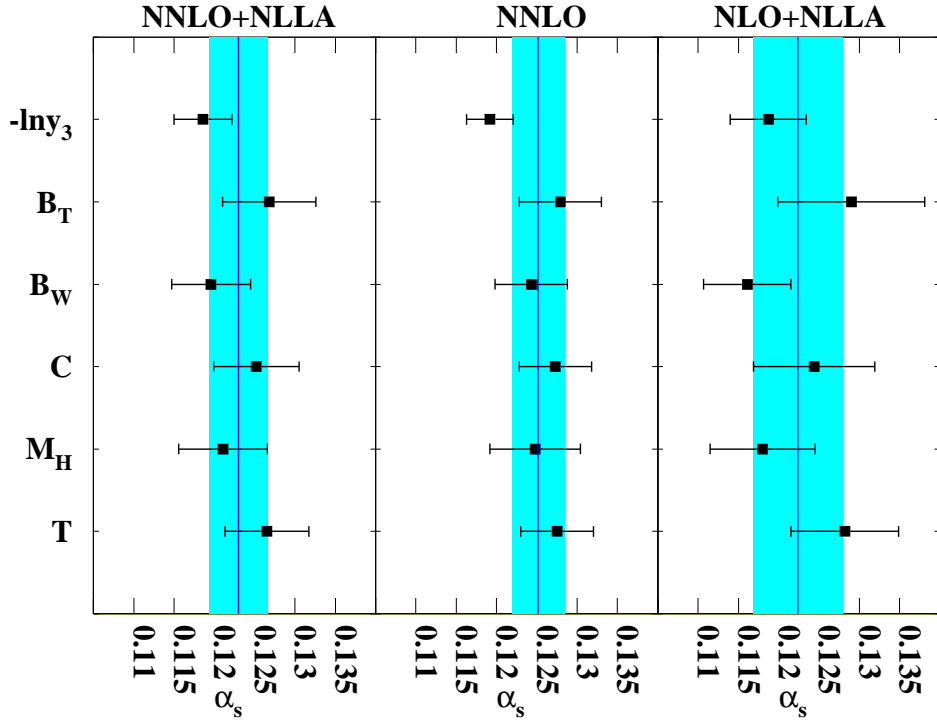


Figure 6: The measurements of the strong coupling constant α_s for the six event shapes, at $\sqrt{s} = M_Z$, when using QCD predictions at different approximations in perturbation theory. The shaded area corresponds to the total uncertainty, as in Fig. 5.

6. Systematic studies

6.1 $\ln R(\mu)$ -matching scheme

As described in section 2, we have computed the two-loop terms proportional to the renormalisation scale in the resummation and matching functions (eq. 2.14) and recomputed the theoretical error in the new matching scheme, which we call the $\ln R(\mu)$ -scheme. It is important to note that this new matching scheme does not affect the central values of

the individual fit results, since the scale $x_\mu = x_L = 1$ is used. Only the perturbative uncertainty will be changed because of the different scale dependence. However, since this uncertainty enters as a weight in the combination procedure, and different event shapes display different scale dependence with the $\ln R(\mu)$ -matching scheme, the central values also change in the combined results. The results for the LEP1 centre-of-mass energy are given in Table 9 for all six variables, whereas the combination of all variables and energies is listed in Table 10. The corresponding uncertainty bands are shown in Fig. 7 for thrust and the three-jet transition variable. It can be seen that in this modified matching scheme the renormalisation scale and x_L dependence are very strongly reduced, leading to a more precise α_s determination. However, given the fact that for a consistent analysis the full NNLLA calculation should be matched to the NNLO prediction, we prefer to quote the values obtained with the standard $\ln R$ -matching as our main result.

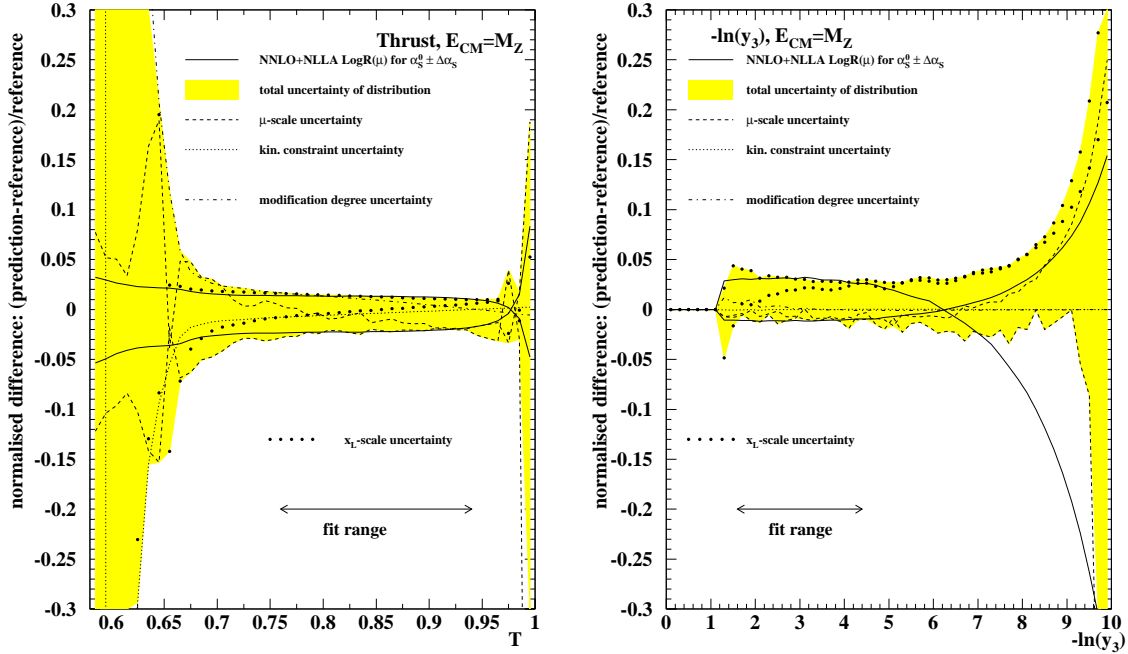


Figure 7: Theoretical uncertainties for the distributions of thrust (left) and the three-jet transition variable (right) at LEP1, using the $\ln R(\mu)$ -matching scheme at NNLO+NLLA.

6.2 Normalisation and quark mass effects

In our nominal analysis the theoretical prediction is normalised to the total hadronic cross section, taking properly into account the production of massive b-quarks. Furthermore, mass corrections are applied for the fixed-order coefficients at leading and next-to-leading order. In order to study the impact of different normalisation and mass correction schemes the analysis has been repeated with alternative options, as summarised in Table 11 for the

LEP1 data. The observed differences when using either the massive or massless hadronic cross section as normalisation are rather minor (first and second row in Table 11). The alternative approach to applying the exact correction $\sigma_0/\sigma_{\text{had}}$, namely expanding this ratio and correspondingly changing the fixed order coefficient functions $B \rightarrow \bar{B}$ and $C \rightarrow \bar{C}$, has been adopted in previous publications. In this case the results are lowered by about 0.5% (third row in Table 11). For completeness, we also give the results obtained with massless coefficients throughout (fourth row in Table 11). This again lowers the result for $\alpha_s(M_Z)$ by 0.5% at LEP1, but has almost no effect at LEP2. The last two rows give the results obtained with different values for the b-quark pole mass, which we use to derive the uncertainty for the mass correction procedure.

6.3 Combination method

Our nominal combination procedure is based on weighted averages with weights proportional to the total significance i.e. $\propto 1/\sigma_{\text{tot}}^2$, where σ_{tot} is the total uncertainty for an individual measurement, thus including the perturbative error in the weight calculation. However, it can be expected that the theoretical uncertainty for a given observable is highly correlated between different energies, the main de-correlation effect being related to the different fit ranges. In contrast, the theoretical uncertainties of different variables at the same energy are clearly less correlated, since missing higher-order contributions are likely to be different. Therefore it is instructive to study the stability of the combination method by using only the largely uncorrelated uncertainty component as weight when combining the results from different energies, while for the first-step combination of different variables at the same energy the theoretical uncertainties are still included. As a result of such a procedure the importance of the statistical error is significantly enhanced, leading to a reduced weight of the LEP2 data with respect to LEP1.

In Table 12, the newly obtained weights are compared to the nominal weights for the combination of measurements at different energies, and the resulting combined measurements are given in Table 13. As anticipated, now the overall combination as well as the resulting theoretical uncertainty are dominated by the LEP1 data, while almost no difference is observed when combining only the LEP2 energy points.

6.4 Hadronisation corrections from NLO+LL event generators

In recent years substantial progress has been achieved in the development of modern Monte Carlo event generators targeted in particular towards the LHC era and often implemented in object oriented C++ frameworks. Compared to the legacy generators used in the LEP era, the new programs include in part NLO corrections matched to parton showers at leading logarithmic accuracy (LL) for various processes. Here we use HERWIG++ [33] version 2.3 for our investigations, which is based on ThePEG [55], a general framework for implementing Monte Carlo generator classes. The nominal version for HERWIG++ uses a LO+LL configuration which features matrix element corrections for the matching of the hard scattering process to the parton showers. Furthermore, two schemes for the implementation of NLO corrections, namely the MCNLO [56] and POWHEG [57] schemes, are

available². The actual implementations of the general NLO to LL matching prescriptions are given in Ref. [58] for MCNLO and in Ref. [59] for POWHEG. Technically, a simulation at NLO+LL is obtained in two steps, where first the NLO partonic configurations are generated [60] and second these events are passed to HERWIG++ to simulate the parton shower, hadronisation and resonance decays.

It should be noted that the nominal LO+LL version with matrix element corrections of HERWIG++ has been extensively tuned to a variety of experimental data, including jet rates, event shapes and particle multiplicities in e^+e^- annihilations from LEP and heavy flavour data from the B-factories [61], in order to obtain the best possible set of parameters. However, according to [61], the quality of this fit, with an overall χ^2 per degree of freedom between 5 and 6, is limited, and this is, to some extent, related to a slightly overestimated amount of gluon radiation in the parton shower. It can not be expected that this tuning is optimal for the NLO+LL versions of HERWIG++. A re-tuning of the parameters using MCNLO and POWHEG is beyond the scope of this paper, but we used parameters suggested in Ref. [62] for MCNLO and checked a few of the main parameters for POWHEG using the ALEPH event shapes [1]. To this end four parameters were individually varied in a simplified grid-search procedure in which for each configuration the χ^2 with respect to the full range of the six event-shape distributions from ALEPH at LEP1 was recorded. This resulted in an improved description of the distributions studied here, presumably at the expense of other distributions included in the more general tuning of HERWIG++.

The following parameters were determined according to this procedure for POWHEG: **AlphaMZ** = 0.134, **cutoffKinScale** = 2.7, **PSplitLight** = 1.1 and **PwtDIquark** = 0.6. The meaning of these parameters can be inferred from [33]. In addition, the partonic configuration was generated with a value of $\Lambda = 170$ MeV to set the scale for the hardest gluon emission according to the evolution in the $\overline{\text{MS}}$ -scheme, yielding $\alpha_s(M_Z)=0.11$.

We compare in a first step the prediction for the event shape distributions of HERWIG++ to both the high precision data at LEP1 from ALEPH and the predictions from the legacy generators PYTHIA, HERWIG and ARIADNE. We recall that the latter have all been tuned to the same global QCD observables measured by ALEPH [51] at LEP1, which included event-shape variables similar to the ones analysed here. In Fig. 8 the generator predictions for thrust, $-\ln(y_3)$ and the total and wide jet broadenings are compared to the ALEPH data.

In general it appears that the shape of HERWIG++ is similar to both HERWIG++ with MCNLO and HERWIG, but all differ in normalisation. A better description is obtained using HERWIG++ with POWHEG. PYTHIA and ARIADNE yield by far the best description. To quantify the performance of the generators, in Table 14 we have compiled the χ^2 of their predictions with respect to the event shapes studied at LEP1, including the experimental systematic uncertainty. A complete re-tuning of the HERWIG++ parameters to the same data used to tune PYTHIA, HERWIG and ARIADNE would likely improve their performance.

To investigate the origin of the observed differences between the generators, it is in-

²We use the notation MCNLO for the *method*, while MC@NLO denotes the *program*.

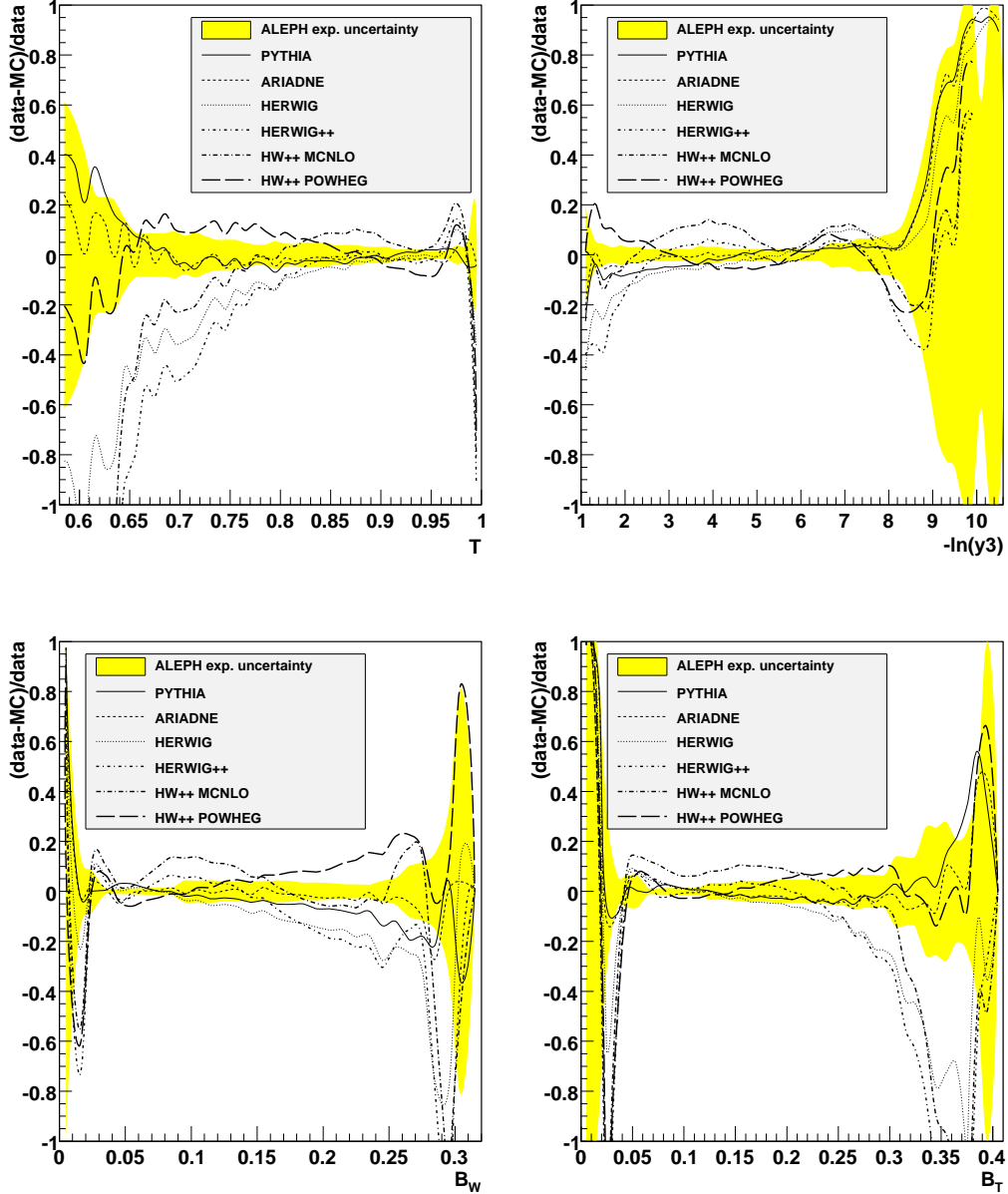


Figure 8: Residuals of hadron level Monte Carlo predictions with respect to the ALEPH data. The shaded area indicates the experimental uncertainty.

structive to consider the parton-level predictions and the hadronisation corrections separately. The parton level predictions from the generators are calculated with final state partons at the end of the parton shower. These are compared to the complete NNLO+NLLA calculation in Fig. 9. For thrust and in particular the total jet broadening a reasonable agreement between NNLO+NLLA and HERWIG++ with POWHEG, as well as a fair agreement with PYTHIA and ARIADNE is observed, while other HERWIG variants show a clear deviation. For $-\ln(y_3)$ and the wide jet broadening all legacy generators provide a

satisfactory description and HERWIG++ based predictions exhibit some systematic differences in shape. It is worth noting that for thrust and the total jet broadening, the PYTHIA prediction overestimates the NNLO+NLLA calculation by about 10%, with the shape in reasonable agreement, whereas a better agreement is seen for the wide jet broadening and $-\ln(y_3)$.

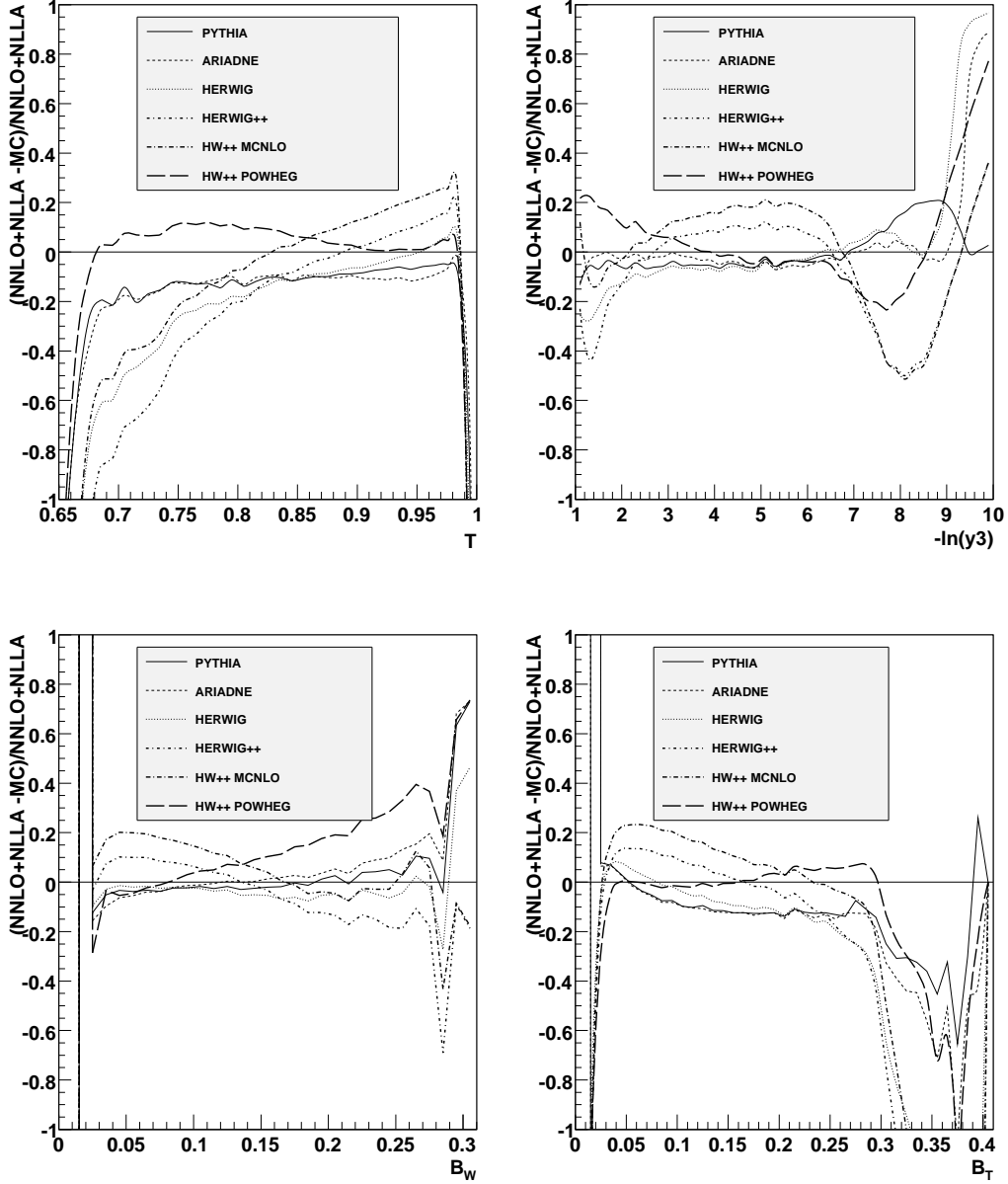


Figure 9: Normalised residuals with respect to the NNLO+NLLA calculation of parton level predictions obtained from different Monte Carlo generators.

The hadronisation corrections to be used in the fits to the data are shown in Fig. 10. HERWIG++ with POWHEG yields a similar shape as the legacy programs, but differs

in the normalisation. The other HERWIG++ predictions differ most notably in shape from the former. In Table 15 the fit results obtained with all generators for hadronisation corrections are given. In most cases, the fits based on HERWIG++ and HERWIG++ with MCNLO are significantly worse than for the other generators, but for individual variables like the wide jet broadening an opposite behaviour is observed. The fit quality of HERWIG++ with POWHEG is similar to the outcome of the legacy generators. Given the similar shape but different normalisation of HERWIG++ with POWHEG, the resulting values of α_s are significantly lower, overall by 3%.

7. Discussion and Conclusions

We have performed a determination of the strong coupling constant α_s from event-shape data measured by the ALEPH collaboration [1], based on the perturbative QCD results at next-to-next-to-leading order (NNLO) matched to resummation in the next-to-leading-logarithmic approximation (NLLA) [24].

Comparing our results to both the fit using purely fixed-order NNLO predictions [27] and the fits based on earlier NLLA+NLO calculations [1], we make the following observations:

- The central value obtained by combining the results for six event-shape variables and the LEP1 and LEP2 centre-of-mass energies,

$$\alpha_s(M_Z) = 0.1224 \pm 0.0009 (\text{stat}) \pm 0.0009 (\text{exp}) \pm 0.0012 (\text{had}) \pm 0.0035 (\text{theo}),$$

is slightly lower than the central value of 0.1228 obtained from fixed-order NNLO only, and slightly larger than the NLO+NLLA results. We note that in this analysis an improved normalisation to the total hadronic cross section has been used, which leads to minor deviations to previously reported results.

The fact that the central value is almost identical to the purely fixed-order NNLO result could be anticipated from the findings in Ref. [24]. There it is shown that in the three-jet region, which provides the bulk of the fit range, the matched NLLA+NNLO prediction is very close to the fixed-order NNLO calculation.

- The dominant theoretical uncertainty on $\alpha_s(M_Z)$, as estimated from scale variations, is reduced by 20% compared to NLO+NLLA. However, compared to the fit based on purely fixed-order NNLO predictions, the perturbative uncertainty is *increased* in the NNLO+NLLA fit. The reason is that in the two-jet region the NLLA+NLO and NLLA+NNLO predictions agree by construction, because the matching suppresses any fixed order terms. Therefore, the renormalisation scale uncertainty is dominated by the next-to-leading-logarithmic approximation in this region, which results in a larger overall scale uncertainty in the α_s fit.
- As already observed for the fixed-order NNLO results, the scatter among the values of $\alpha_s(M_Z)$ extracted from the six different event-shape variables is smaller than in the NLO+NLLA case.

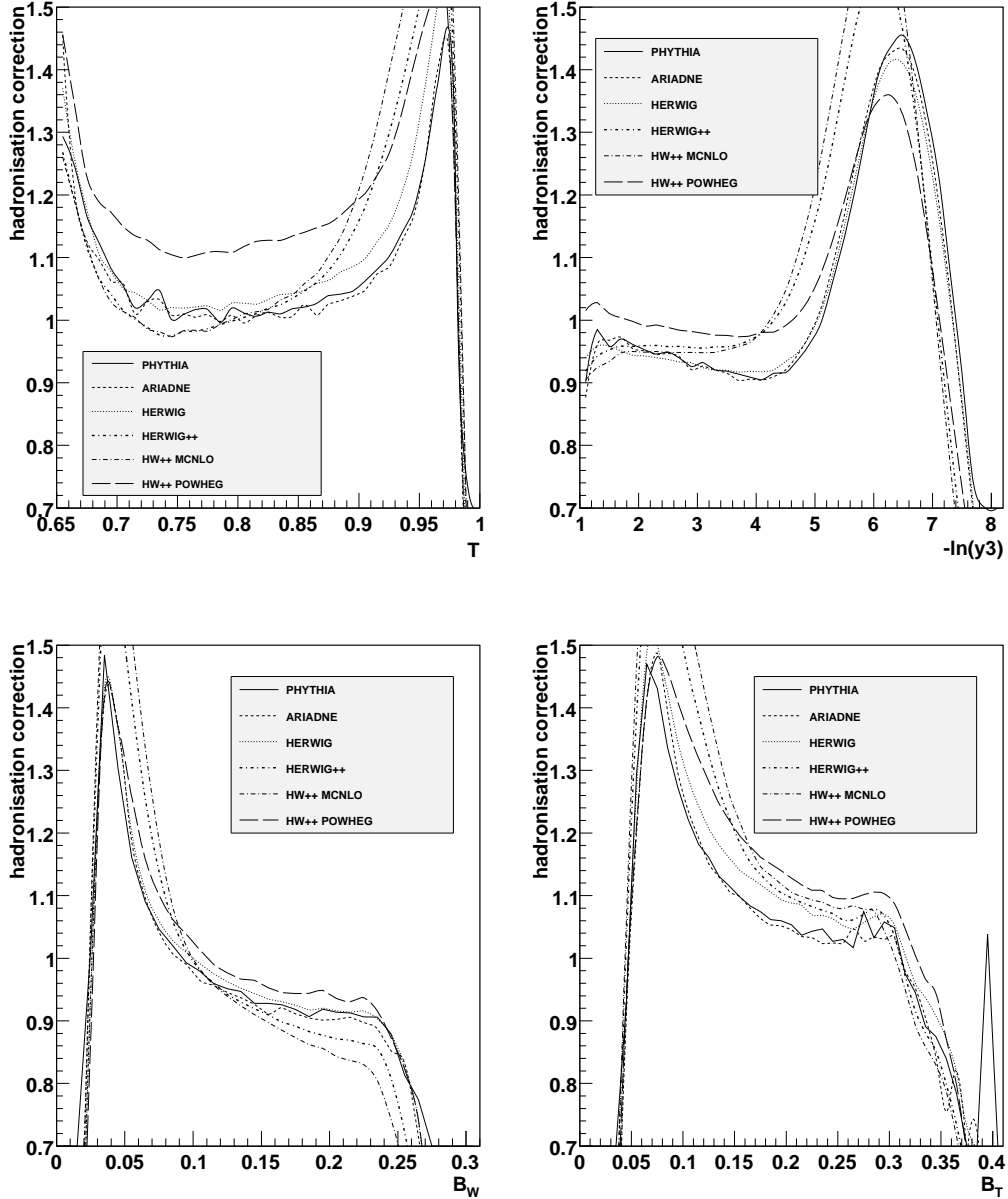


Figure 10: Hadronisation corrections (ratio of hadron to parton level predictions) obtained from different Monte Carlo generators.

- The matching of NLLA+NNLO introduces a mismatch in the cancellation of renormalisation scale logarithms, since the NNLO expansion fully compensates the renormalisation scale dependence up to two loops, while NLLA only compensates it up to one loop. In order to assess the impact of this mismatch, we introduced the $\ln R(\mu)$ matching scheme, which retains the two-loop renormalisation terms in the resummed expressions and the matching coefficients. In this scheme, a substantial reduction of the perturbative uncertainty from ± 0.0035 (obtained in the default $\ln R$ -scheme) to

± 0.0022 is observed, which might indicate the size of the ultimately reachable precision for a complete NNLO+NNLLA calculation including the currently unknown resummed function g_3 for all shape variables. Although both schemes are in principle on the same theoretical footing, it is the more conservative error estimate obtained in the $\ln R$ -scheme which should be taken as the nominal value, since it measures the potential impact of the yet uncalculated finite NNLLA-terms.

- Bottom quark mass effects, which are numerically significant mainly at the LEP1 energy, were included through to NLO. Compared to a purely massless evaluation of the distributions, the inclusion of these mass effects enhances $\alpha_s(M_Z)$ by 0.8%. Compared to the previously used expansion of the mass corrections, an enhancement of 0.4% is observed.
- The averaging of $\alpha_s(M_Z)$ values obtained at the various LEP1 and LEP2 energies weights the different measurements by their total uncertainties. Excluding the error on the perturbative prediction from this weighting enhances the importance of the very precise LEP1 data over the LEP2 data, and yields an $\alpha_s(M_Z)$ value which is lower than our default result by only 0.2%, thereby demonstrating the very good consistency of the LEP1 and LEP2 results.
- We have investigated hadronisation corrections obtained from NLO+LL parton shower simulation using HERWIG++ with two different schemes. Results for α_s based on corrections from HERWIG++ with POWHEG are slightly lower than with nominal corrections from PYTHIA. Comparing hadron level predictions with data reveals that HERWIG++ with POWHEG yields an improved prediction over HERWIG, HERWIG++ and HERWIG++ with MCNLO, but does not reach the same level of agreement as PYTHIA and ARIADNE. Further, we observe a certain discrepancy between MCNLO and POWHEG, which might indicate unresolved tuning issues. Therefore, while the first studies with HERWIG++ look rather promising, we retain for the time being PYTHIA as generator for our nominal result.
- From the study of hadronisation corrections we also make the following important observation. It appears that there are two “classes” of variables. The first class contains thrust, C-parameter and total jet broadening, whereas the second class consists of the heavy jet mass, wide jet broadening and the two-to-three-jet transition parameter $-\ln y_3$. For the first class, using the standard hadronisation corrections from PYTHIA, we obtain $\alpha_s(M_Z)$ values around $0.125 - 0.127$, some 5% higher than those found from the second class of variables. In a study of higher moments of event shapes [32], indications were found that variables from the first class still exhibit sizable missing higher order corrections, whereas the second class of observables have a better perturbative stability. In this paper, from Fig. 9, we observe that this first class of variables gives a parton level prediction with PYTHIA, which is about 10% higher than the NNLO+NLLA prediction. The PYTHIA curve is obtained with tuned parameters, where the tuning to data had been performed at the hadron

level. Indeed, this tuning results in a rather large effective coupling in the parton shower, which might partly explain the larger parton level prediction of PYTHIA. However, since the tuning has been performed at hadron level, this implies that the hadronisation corrections come out to be smaller than what would have been found by tuning a hypothetical Monte Carlo prediction with a parton level corresponding to the NNLO+NLLA prediction. Thus, in the end, the PYTHIA hadronisation corrections, applied in the α_s fit, might be too small, resulting in a larger $\alpha_s(M_Z)$ value. Such problems do not appear to exist for the second class of variables.

In summary, there are indications that the first class of event shapes still suffers from significant missing higher order contributions, even beyond NNLO+NLLA. This might also have led to a tuning of parton shower models which underestimates the hadronisation corrections for these variables, and consequently results in somewhat larger values of the fitted strong coupling. Since up to now the hadronisation uncertainties have been estimated from the differences of parton shower based models, tuned to the data, it is likely that for these event shapes the uncertainties were underestimated and not able to account for a possible systematic shift.

In future work it would be interesting to investigate the effect of NNLLA resummation terms for all six event shapes, of electroweak corrections, of quark mass effects beyond NLO and of non-perturbative power-law corrections as well as further studies with HERWIG++, in particular using the newly developed improved algorithm for merging matrix elements with angular-ordered parton showers [63].

Acknowledgements

We wish to thank the authors of HERWIG++ for fruitful discussions on hadronisation corrections and O. Latunde-Dada for valuable instructions on running the MCPWNLO interface. GH and HS would like to thank the Institute for Theoretical Physics, University of Zürich, for hospitality while part of this work was carried out. EWNG gratefully acknowledges the support of the Wolfson Foundation and the Royal Society. This research was supported in part by the Swiss National Science Foundation (SNF) under contracts PP0022-118864 and 200020-117602, by the UK Science and Technology Facilities Council, by the European Commission’s Marie-Curie Research Training Network under contract MRTN-CT-2006-035505 “Tools and Precision Calculations for Physics Discoveries at Colliders” and by the German Helmholtz Alliance “Physics at the Terascale”.

References

- [1] A. Heister *et al.* [ALEPH Collaboration], *Eur. Phys. J. C* **35** (2004) 457.
- [2] D. Buskulic *et al.* [ALEPH Collaboration], *Z. Phys. C* **73** (1997) 409.
- [3] P.D. Acton *et al.* [OPAL Collaboration], *Z. Phys. C* **59** (1993) 1;
 G. Alexander *et al.* [OPAL Collaboration], *Z. Phys. C* **72** (1996) 191;
 K. Ackerstaff *et al.* [OPAL Collaboration], *Z. Phys. C* **75** (1997) 193;

- G. Abbiendi *et al.* [OPAL Collaboration], Eur. Phys. J. C **16** (2000) 185 [hep-ex/0002012];
 G. Abbiendi *et al.* [OPAL Collaboration], Eur. Phys. J. C **40** (2005) 287 [hep-ex/0503051].
 G. Abbiendi *et al.* [OPAL Collaboration], Eur. Phys. J. C **53** (2008) 21.
- [4] M. Acciarri *et al.* [L3 Collaboration], Phys. Lett. B **371** (1996) 137;
 M. Acciarri *et al.* [L3 Collaboration], Phys. Lett. B **404** (1997) 390;
 M. Acciarri *et al.* [L3 Collaboration], Phys. Lett. B **444** (1998) 569;
 P. Achard *et al.* [L3 Collaboration], Phys. Lett. B **536** (2002) 217 [hep-ex/0206052];
 P. Achard *et al.* [L3 Collaboration], Phys. Rept. **399** (2004) 71 [hep-ex/0406049].
- [5] P. Abreu *et al.* [DELPHI Collaboration], Phys. Lett. B **456** (1999) 322;
 J. Abdallah *et al.* [DELPHI Collaboration], Eur. Phys. J. C **29** (2003) 285 [hep-ex/0307048];
 J. Abdallah *et al.* [DELPHI Collaboration], Eur. Phys. J. C **37** (2004) 1 [hep-ex/0406011].
- [6] K. Abe *et al.* [SLD Collaboration], Phys. Rev. D **51** (1995) 962 [hep-ex/9501003].
- [7] P.A. Movilla Fernandez, O. Biebel, S. Bethke, S. Kluth and P. Pfeifenschneider [JADE Collaboration], Eur. Phys. J. C **1** (1998) 461 [hep-ex/9708034];
 P. Pfeifenschneider *et al.* [JADE collaboration], Eur. Phys. J. C **17** (2000) 19 [hep-ex/0001055].
- [8] R.K. Ellis, D.A. Ross and A.E. Terrano, Nucl. Phys. B **178** (1981) 421.
- [9] Z. Kunszt, Phys. Lett. B **99** (1981) 429;
 J.A.M. Vermaseren, K.J.F. Gaemers and S.J. Oldham, Nucl. Phys. B **187** (1981) 301;
 K. Fabricius, I. Schmitt, G. Kramer and G. Schierholz, Z. Phys. C **11** (1981) 315.
- [10] Z. Kunszt and P. Nason, in *Z Physics at LEP 1*, CERN Yellow Report 89-08, Vol. 1, p. 373;
 W. T. Giele and E.W.N. Glover, Phys. Rev. D **46** (1992) 1980;
 S. Catani and M. H. Seymour, Phys. Lett. B **378** (1996) 287 [hep-ph/9602277].
- [11] A. Gehrmann-De Ridder, T. Gehrmann, E.W.N. Glover and G. Heinrich, Phys. Rev. Lett. **99** (2007) 132002 [arXiv:0707.1285].
- [12] A. Gehrmann-De Ridder, T. Gehrmann, E.W.N. Glover and G. Heinrich, JHEP **0711** (2007) 058 [arXiv:0710.0346]; Phys. Rev. Lett. **100** (2008) 172001 [arXiv:0802.0813].
- [13] A. Gehrmann-De Ridder, T. Gehrmann, E.W.N. Glover and G. Heinrich, JHEP **0712** (2007) 094 [arXiv:0711.4711].
- [14] S. Weinzierl, Phys. Rev. Lett. **101** (2008) 162001 [arXiv:0807.3241].
- [15] S. Weinzierl, arXiv:0904.1077.
- [16] S. Weinzierl, arXiv:0904.1145.
- [17] S. Brandt, C. Peyrou, R. Sosnowski and A. Wroblewski, Phys. Lett. **12** (1964) 57;
 E. Farhi, Phys. Rev. Lett. **39** (1977) 1587.
- [18] L. Clavelli and D. Wyler, Phys. Lett. B **103** (1981) 383.
- [19] P.E.L. Rakow and B.R. Webber, Nucl. Phys. B **191** (1981) 63.
- [20] G. Parisi, Phys. Lett. B **74** (1978) 65;
 J.F. Donoghue, F.E. Low and S.Y. Pi, Phys. Rev. D **20** (1979) 2759.

- [21] S. Catani, Y.L. Dokshitzer, M. Olsson, G. Turnock and B.R. Webber, Phys. Lett. B **269** (1991) 432;
 N. Brown and W.J. Stirling, Phys. Lett. B **252** (1990) 657; Z. Phys. C **53** (1992) 629;
 W.J. Stirling *et al.*, Proceedings of the Durham Workshop, J. Phys. **G17** (1991) 1567;
 S. Bethke, Z. Kunszt, D.E. Soper and W.J. Stirling, Nucl. Phys. B **370** (1992) 310
 [Erratum-ibid. B **523** (1998) 681].
- [22] R.W.L. Jones, M. Ford, G.P. Salam, H. Stenzel and D. Wicke, JHEP **0312** (2003) 007
 [hep-ph/0312016].
- [23] S. Catani, L. Trentadue, G. Turnock and B.R. Webber, Nucl. Phys. B **407** (1993) 3.
- [24] T. Gehrmann, G. Luisoni and H. Stenzel, Phys. Lett. B **664** (2008) 265 [arXiv:0803.0695].
- [25] T. Becher and M.D. Schwartz, JHEP **0807** (2008) 034 [arXiv:0803.0342].
- [26] S. Fleming, A.H. Hoang, S. Mantry and I.W. Stewart, Phys. Rev. D **77** (2008) 074010
 [hep-ph/0703207]; Phys. Rev. D **77** (2008) 114003 [arXiv:0711.2079];
 M.D. Schwartz, Phys. Rev. D **77** (2008) 014026 [arXiv:0709.2709];
 C.W. Bauer, S.P. Fleming, C. Lee and G. Sterman, arXiv:0801.4569.
- [27] G. Dissertori, A. Gehrmann-De Ridder, T. Gehrmann, E.W.N. Glover, G. Heinrich and
 H. Stenzel, JHEP **0802** (2008) 040 [arXiv:0712.0327].
- [28] S. Bethke, S. Kluth, C. Pahl and J. Schieck [JADE Collaboration], arXiv:0810.1389.
- [29] R. A. Davison and B. R. Webber, Eur. Phys. J. C **59** (2009) 13 [arXiv:0809.3326].
- [30] C. Pahl, S. Bethke, S. Kluth, J. Schieck and the JADE collaboration, Eur. Phys. J. C **60**
 (2009) 181 [arXiv:0810.2933].
- [31] C. Pahl, S. Bethke, O. Biebel, S. Kluth and J. Schieck, arXiv:0904.0786.
- [32] A. Gehrmann-De Ridder, T. Gehrmann, E.W.N. Glover and G. Heinrich, JHEP **0905** (2009)
 106 [arXiv:0903.4658].
- [33] M. Bähr *et al.*, Eur. Phys. J. C **58** (2008) 639 [arXiv:0803.0883];
 M. Bähr *et al.*, arXiv:0812.0529.
- [34] W. Bernreuther, A. Brandenburg and P. Uwer, Phys. Rev. Lett. **79** (1997) 189
 [hep-ph/9703305];
 A. Brandenburg and P. Uwer, Nucl. Phys. B **515** (1998) 279 [hep-ph/9708350];
 G. Rodrigo, A. Santamaria and M.S. Bilenky, Phys. Rev. Lett. **79** (1997) 193
 [hep-ph/9703358];
 P. Nason and C. Oleari, Nucl. Phys. B **521** (1998) 237 [hep-ph/9709360].
- [35] L.W. Garland, T. Gehrmann, E.W.N. Glover, A. Koukoutsakis and E. Remiddi, Nucl. Phys.
 B **627** (2002) 107 [hep-ph/0112081] and **642** (2002) 227 [hep-ph/0206067].
- [36] S. Moch, P. Uwer and S. Weinzierl, Phys. Rev. D **66** (2002) 114001 [hep-ph/0207043].
- [37] E.W.N. Glover and D.J. Miller, Phys. Lett. B **396** (1997) 257 [hep-ph/9609474];
 Z. Bern, L.J. Dixon, D.A. Kosower and S. Weinzierl, Nucl. Phys. B **489** (1997) 3
 [hep-ph/9610370];
 J.M. Campbell, E.W.N. Glover and D.J. Miller, Phys. Lett. B **409** (1997) 503
 [hep-ph/9706297];
 Z. Bern, L.J. Dixon and D.A. Kosower, Nucl. Phys. B **513** (1998) 3 [hep-ph/9708239].

- [38] K. Hagiwara and D. Zeppenfeld, Nucl. Phys. B **313** (1989) 560;
F.A. Berends, W.T. Giele and H. Kuijf, Nucl. Phys. B **321** (1989) 39;
N.K. Falck, D. Graudenz and G. Kramer, Nucl. Phys. B **328** (1989) 317.
- [39] A. Gehrmann-De Ridder, T. Gehrmann and E.W.N. Glover, JHEP **0509** (2005) 056
[hep-ph/0505111]; Nucl. Phys. B **691** (2004) 195 [hep-ph/0403057]; Phys. Lett. B **612** (2005)
36 [hep-ph/0501291]; **612** (2005) 49 [hep-ph/0502110].
- [40] R. Barate *et al.* [ALEPH Collaboration], Eur. Phys. J. C **18** (2000) 1 [hep-ex/0008013].
- [41] K. G. Chetyrkin, A. L. Kataev and F. V. Tkachov, Phys. Lett. B **85** (1979) 277;
W. Celmaster and R. J. Gonsalves, Phys. Rev. Lett. **44** (1980) 560;
M. Dine and J. R. Sapiirstein, Phys. Rev. Lett. **43**, 668 (1979);
K.G. Chetyrkin, J.H. Kühn and A. Kwiatkowski, Phys. Rept. **277** (1996) 189.
- [42] A. Denner, S. Dittmaier, T. Gehrmann and C. Kurz, arXiv:0906.0372.
- [43] C. M. Carloni-Calame, S. Moretti, F. Piccinini and D. A. Ross, JHEP **0903** (2009) 047
[arXiv:0804.3771].
- [44] S. Catani, G. Turnock, B.R. Webber and L. Trentadue, Phys. Lett. B **263** (1991) 491.
- [45] S. Catani, G. Turnock and B.R. Webber, Phys. Lett. B **272** (1991) 368;
E. Gardi and J. Rathsmann, Nucl. Phys. B **638** (2002) 243 [hep-ph/0201019].
- [46] S. Catani, G. Turnock and B.R. Webber, Phys. Lett. B **295** (1992) 269.
- [47] Y.L. Dokshitzer, A. Lucenti, G. Marchesini and G.P. Salam, JHEP **9801** (1998) 011
[hep-ph/9801324].
- [48] S. Catani and B. R. Webber, Phys. Lett. B **427** (1998) 377 [hep-ph/9801350];
E. Gardi and L. Magnea, JHEP **0308** (2003) 030 [hep-ph/0306094].
- [49] A. Banfi, G.P. Salam and G. Zanderighi, JHEP **0201** (2002) 018 [hep-ph/0112156].
- [50] M. Dasgupta and G.P. Salam, J. Phys. G **30** (2004) R143 [hep-ph/0312283].
- [51] R. Barate *et al.* [ALEPH Collaboration], Phys. Rep. **294** (1998) 1.
- [52] T. Sjostrand, P. Eden, C. Friberg, L. Lönnblad, G. Miu, S. Mrenna and E. Norrbin, Comput.
Phys. Commun. **135** (2001) 238 [hep-ph/0010017].
- [53] G. Corcella *et al.*, JHEP **0101** (2001) 010 [hep-ph/0011363].
- [54] L. Lönnblad, Comput. Phys. Commun. **71** (1992) 15.
- [55] L. Lönnblad, Comput. Phys. Commun. **118** (1999) 213 [hep-ph/9810208].
- [56] S. Frixione and B. R. Webber, JHEP **0206** (2002) 029 [hep-ph/0204244].
- [57] P. Nason, JHEP **0411** (2004) 040 [hep-ph/0409146].
- [58] O. Latunde-Dada, JHEP **0711** (2007) 040 [arXiv:0708.4390].
- [59] O. Latunde-Dada, S. Gieseke and B. Webber, JHEP **0702** (2007) 051 [hep-ph/0612281].
- [60] O. Latunde-Dada, MCPWNLO program, private communication.
- [61] S. Gieseke, P. Stephens and B. Webber, JHEP **0312** (2003) 045 [hep-ph/0310083] and
references therein.
- [62] O. Latunde-Dada, private communication.
- [63] K. Hamilton, P. Richardson and J. Tully, arXiv:0905.3072.

$Q = 91.2 \text{ GeV}$						
variable	T	$-\ln y_3$	M_H	C	B_W	B_T
α_s	0.1265	0.1186	0.1211	0.1252	0.1196	0.1268
stat. error	0.0002	0.0002	0.0003	0.0002	0.0002	0.0002
exp. error	0.0008	0.0011	0.0010	0.0007	0.0007	0.0007
pert. error	0.0048	0.0029	0.0033	0.0050	0.0046	0.0053
hadr. error	0.0019	0.0017	0.0042	0.0016	0.0017	0.0022
total error	0.0052	0.0036	0.0055	0.0053	0.0049	0.0058
fit range	0.75-0.91	1.6-4.0	0.10-0.22	0.36-0.74	0.09-0.19	0.16-0.30
$Q = 133 \text{ GeV}$						
variable	T	$-\ln y_3$	M_H	C	B_W	B_T
α_s	0.1193	0.1199	0.1149	0.1174	0.1158	0.1205
stat. error	0.0047	0.0057	0.0053	0.0037	0.0032	0.0031
exp. error	0.0006	0.0004	0.0012	0.0008	0.0008	0.0010
pert. error	0.0039	0.0024	0.0027	0.0040	0.0038	0.0044
hadr. error	0.0015	0.0010	0.0027	0.0012	0.0010	0.0013
total error	0.0063	0.0063	0.0067	0.0057	0.0051	0.0056
fit range	0.75-0.94	1.6-4.4	0.08-0.25	0.30-0.75	0.08-0.25	0.13-0.35
$Q = 161 \text{ GeV}$						
variable	T	$-\ln y_3$	M_H	C	B_W	B_T
α_s	0.1172	0.1183	0.1225	0.1190	0.1186	0.1238
stat. error	0.0080	0.0082	0.0072	0.0066	0.0047	0.0052
exp. error	0.0006	0.0004	0.0012	0.0008	0.0008	0.0010
pert. error	0.0036	0.0022	0.0025	0.0037	0.0035	0.0040
hadr. error	0.0014	0.0007	0.0022	0.0011	0.0008	0.0010
total error	0.0088	0.0085	0.0079	0.0076	0.0060	0.0067
fit range	0.75-0.94	1.6-4.4	0.08-0.25	0.30-0.75	0.08-0.25	0.13-0.35
$Q = 172 \text{ GeV}$						
variable	T	$-\ln y_3$	M_H	C	B_W	B_T
α_s	0.1120	0.1095	0.1079	0.1093	0.1036	0.1108
stat. error	0.0077	0.0098	0.0085	0.0063	0.0063	0.0069
exp. error	0.0006	0.0006	0.0012	0.0008	0.0008	0.0012
pert. error	0.0035	0.0021	0.0024	0.0035	0.0033	0.0039
hadr. error	0.0013	0.0006	0.0020	0.0010	0.0007	0.0010
total error	0.0085	0.0100	0.0091	0.0074	0.0072	0.0081
fit range	0.75-0.94	1.6-4.4	0.08-0.25	0.22-0.75	0.08-0.25	0.11-0.35

Table 1: Results for $\alpha_s(Q)$ as obtained from NNLO+NLLA fits to distributions of event-shape variables at $Q = \sqrt{s} = 91.2, 133, 161$ and 172 GeV .

$Q = 183 \text{ GeV}$						
variable	T	$-\ln y_3$	M_H	C	B_W	B_T
α_s	0.1131	0.1083	0.1129	0.1094	0.1091	0.1148
stat. error	0.0036	0.0050	0.0038	0.0032	0.0027	0.0030
exp. error	0.0007	0.0007	0.0012	0.0011	0.0008	0.0011
pert. error	0.0034	0.0021	0.0023	0.0034	0.0033	0.0037
hadr. error	0.0013	0.0005	0.0018	0.0010	0.0007	0.0010
total error	0.0051	0.0055	0.0050	0.0049	0.0043	0.0050
fit range	0.80-0.96	2.4-4.8	0.06-0.20	0.22-0.60	0.065-0.20	0.11-0.30
$Q = 189 \text{ GeV}$						
variable	T	$-\ln y_3$	M_H	C	B_W	B_T
α_s	0.1119	0.1087	0.1087	0.1121	0.1056	0.1137
stat. error	0.0026	0.0031	0.0032	0.0018	0.0019	0.0019
exp. error	0.0007	0.0005	0.0017	0.0009	0.0009	0.0012
pert. error	0.0033	0.0020	0.0023	0.0034	0.0032	0.0037
hadr. error	0.0012	0.0005	0.0018	0.0010	0.0006	0.0010
total error	0.0045	0.0038	0.0046	0.0040	0.0039	0.0044
fit range	0.80-0.96	2.4-4.8	0.06-0.20	0.22-0.60	0.065-0.20	0.11-0.30
$Q = 200 \text{ GeV}$						
variable	T	$-\ln y_3$	M_H	C	B_W	B_T
α_s	0.1078	0.1065	0.1020	0.1109	0.1047	0.1081
stat. error	0.0027	0.0032	0.0034	0.0021	0.0019	0.0024
exp. error	0.0007	0.0005	0.0019	0.0008	0.0008	0.0013
pert. error	0.0032	0.0020	0.0023	0.0033	0.0032	0.0036
hadr. error	0.0012	0.0005	0.0016	0.0009	0.0006	0.0010
total error	0.0045	0.0038	0.0048	0.0041	0.0039	0.0046
fit range	0.80-0.96	2.4-4.8	0.06-0.20	0.22-0.60	0.065-0.20	0.11-0.30
$Q = 206 \text{ GeV}$						
variable	T	$-\ln y_3$	M_H	C	B_W	B_T
α_s	0.1084	0.1040	0.1076	0.1076	0.1051	0.1089
stat. error	0.0025	0.0032	0.0024	0.0019	0.0017	0.0020
exp. error	0.0007	0.0005	0.0012	0.0008	0.0008	0.0011
pert. error	0.0032	0.0020	0.0022	0.0033	0.0031	0.0035
hadr. error	0.0012	0.0004	0.0016	0.0009	0.0006	0.0010
total error	0.0043	0.0038	0.0039	0.0040	0.0037	0.0043
fit range	0.80-0.96	2.4-4.8	0.04-0.20	0.22-0.60	0.05-0.20	0.11-0.30

Table 2: Results for $\alpha_s(Q)$ as obtained from NNLO+NLLA fits to distributions of event-shape variables at $Q = \sqrt{s} = 183, 189, 200$ and 206 GeV .

	T	C	M_H	B_W	B_T	$-\ln y_3$
NNLO+NLLA	0.1266	0.1252	0.1211	0.1196	0.1268	0.1186
χ^2/N_{dof}	0.16	0.47	4.4	4.4	0.84	1.89
stat.error	0.0002	0.0002	0.0003	0.0002	0.0002	0.0002
NLO+NLLA	0.1282	0.1244	0.1180	0.1161	0.1290	0.1187
χ^2/N_{dof}	0.74	1.88	14.5	19.6	9.7	4.7
stat.error	0.0002	0.0002	0.0003	0.0002	0.0002	0.0002
NNLO	0.1275	0.1273	0.1248	0.1242	0.1279	0.1192
χ^2/N_{dof}	1.16	1.08	4.1	2.74	0.50	1.17
stat.error	0.0002	0.0002	0.0004	0.0002	0.0002	0.0003
fit range	0.75 - 0.91	0.36 - 0.74	0.10 - 0.22	0.09 - 0.19	0.16 - 0.30	1.6-4.0

Table 3: Fit results for $\alpha_s(M_Z)$ using different predictions of perturbative QCD, with the renormalisation scale fixed to $\mu = M_Z$.

Q [GeV]	91.2	133	161	172	183	189	200	206
$\alpha_s(Q)$	0.1221	0.1179	0.1201	0.1086	0.1112	0.1099	0.1067	0.1066
stat. error	0.0001	0.0029	0.0043	0.0052	0.0023	0.0016	0.0017	0.0015
exp. error	0.0008	0.0008	0.0008	0.0008	0.0009	0.0009	0.0008	0.0009
pert. error	0.0041	0.0036	0.0033	0.0032	0.0031	0.0030	0.0029	0.0029
had. error	0.0018	0.0012	0.0010	0.0010	0.0009	0.0008	0.0008	0.0008
total error	0.0045	0.0049	0.0056	0.0062	0.0040	0.0036	0.0036	0.0034
RMS	0.0038	0.0023	0.0026	0.0029	0.0027	0.0030	0.0030	0.0019

Table 4: Combined results for $\alpha_s(Q)$ using NNLO+NLLA predictions.

Q [GeV]	91.2	133	161	172	183	189	200	206
$\alpha_s(M_Z)$	0.1221	0.1251	0.1316	0.1190	0.1235	0.1225	0.1196	0.1200
stat. error	0.0001	0.0033	0.0052	0.0063	0.0028	0.0020	0.0022	0.0019
exp. error	0.0008	0.0010	0.0010	0.0011	0.0011	0.0011	0.0011	0.0011
pert. error	0.0041	0.0038	0.0036	0.0035	0.0034	0.0033	0.0033	0.0032
had. error	0.0018	0.0014	0.0012	0.0011	0.0011	0.0010	0.0010	0.0010
total error	0.0045	0.0053	0.0065	0.0074	0.0047	0.0042	0.0042	0.0041
RMS	0.0038	0.0026	0.0032	0.0035	0.0033	0.0037	0.0038	0.0024

Table 5: Combined results for $\alpha_s(M_Z)$ using NNLO+NLLA predictions.

Q [GeV]	91.2	133	161	172	183	189	200	206
$\alpha_s(M_Z)$	0.1239	0.1270	0.1313	0.1192	0.1226	0.1234	0.1200	0.1202
stat. error	0.0002	0.0033	0.0051	0.0063	0.0028	0.0020	0.0021	0.0019
exp. error	0.0009	0.0009	0.0009	0.0010	0.0010	0.0010	0.0010	0.0010
pert. error	0.0030	0.0030	0.0028	0.0028	0.0027	0.0026	0.0025	0.0025
hadr. error	0.0018	0.0014	0.0012	0.0012	0.0011	0.0010	0.0010	0.0010
total error	0.0037	0.0048	0.0060	0.0070	0.0041	0.0036	0.0036	0.0034
RMS	0.0036	0.0014	0.0043	0.0019	0.0027	0.0027	0.0034	0.0024

Table 6: Combined results for $\alpha_s(M_Z)$ using NNLO predictions.

data set	LEP1 + LEP2	LEP2
$\alpha_s(M_Z)$	0.1224	0.1224
stat. error	0.0009	0.0011
exp. error	0.0009	0.0010
pert. error	0.0035	0.0034
hadr. error	0.0012	0.0011
total error	0.0039	0.0039

Table 7: Weighted average of combined measurements for $\alpha_s(M_Z)$ obtained at energies from 91.2 GeV to 206 GeV and the average without the point at $\sqrt{s} = M_Z$ using NNLO+NLLA predictions.

theory input	NNLO+NLLA	NNLO	NLO+NLLA
$\alpha_s(M_Z)$	0.1224	0.1228	0.1215
stat. error	0.0009	0.0008	0.0010
exp. error	0.0009	0.0009	0.0009
pert. error	0.0035	0.0027	0.0053
hadr. error	0.0012	0.0012	0.0012
total error	0.0039	0.0032	0.0056

Table 8: Comparison of combined results obtained with different theoretical predictions on $\alpha_s(M_Z)$ using ALEPH data at energies from 91.2 GeV to 206 GeV.

variable	T	$-\ln y_3$	M_H	C	B_W	B_T
$\ln R(\mu)$	0.0017	0.0028	0.0025	0.0030	0.0031	0.0025
$\ln R$	0.0047	0.0029	0.0033	0.0049	0.0045	0.0053

Table 9: Comparison of the theoretical systematic uncertainties for the $\ln R$ and $\ln R(\mu)$ matching schemes. Only the uncertainty for missing higher orders as obtained from the uncertainty band method are included, using $\alpha_s(M_Z)=0.1224$. The total perturbative uncertainty also accounts for the mass corrections, the latter are the same for both matching schemes.

data set	LEP1 + LEP2	LEP2
$\alpha_s(M_Z)$	0.1227	0.1226
stat. error	0.0008	0.0010
exp. error	0.0009	0.0010
pert. error	0.0022	0.0021
hadr. error	0.0012	0.0011
total error	0.0028	0.0028

Table 10: Weighted average of combined measurements for $\alpha_s(M_Z)$, obtained at energies from 91.2 GeV to 206 GeV and without the point at $\sqrt{s} = M_Z$, using in all cases the $\ln R(\mu)$ matching scheme.

variable	T	$-\ln y_3$	M_H	C	B_W	B_T
σ_{had} (massive)	0.1266	0.1186	0.1211	0.1252	0.1196	0.1268
σ_{had} (massless)	0.1266	0.1187	0.1212	0.1252	0.1196	0.1268
massless expansion, massive A, B	0.1260	0.1183	0.1208	0.1247	0.1192	0.1262
massless expansion, massless A, B	0.1256	0.1179	0.1215	0.1242	0.1188	0.1253
σ_{had} (massive, $M_b = 4.0 \text{ GeV}/c^2$)	0.1264	0.1185	0.1212	0.1251	0.1195	0.1267
σ_{had} (massive, $M_b = 5.0 \text{ GeV}/c^2$)	0.1268	0.1189	0.1210	0.1252	0.1198	0.1270

Table 11: Results on $\alpha_s(M_Z)$ from LEP1 data using different normalisation and mass correction schemes.

Q [GeV]	91.2	133	161	172	183	189	200	206
with pert.err.	14.0	10.3	6.8	5.3	13.1	16.7	16.4	17.5
w/o pert.err.	80.0	2.5	2.6	2.5	2.8	3.1	3.2	3.3

Table 12: Weights (in per cent) of the different centre-of-mass energy points in the global combination, with and without the inclusion of theoretical uncertainties.

data set	LEP1 + LEP2	LEP2
$\alpha_s(M_Z)$	0.1222	0.1228
stat. error	0.0003	0.0013
exp. error	0.0007	0.0010
pert. error	0.0039	0.0034
hadr. error	0.0017	0.0011
total error	0.0044	0.0040

Table 13: Weighted average of the combined measurements for $\alpha_s(M_Z)$, based on weights which do not include the theoretical uncertainty.

	T	C	M_H	B_W	B_T	$-\ln y_3$	global
PYTHIA	0.55	1.05	1.9	2.5	0.57	1.31	1.30
ARIADNE	0.44	0.75	0.60	0.97	0.58	0.52	0.65
HERWIG	6.9	5.3	9.4	9.8	4.4	4.0	6.6
HW++	17.5	16.5	18.2	13.4	9.4	5.6	13.5
HW++ MCNLO	9.6	15.9	9.2	10.5	11.8	5.5	10.4
HW++ POWHEG	3.9	11.2	8.5	6.9	3.5	2.3	6.1

Table 14: Comparison of hadron level predictions from various event generators to the ALEPH event-shape data. The Table shows the χ^2 values normalised to the number of experimental bins, including statistical and experimental systematic uncertainties of the data.

$\alpha_s(M_Z)$	T	C	M_H	B_W	B_T	$-\ln y_3$
PYTHIA	0.1266	0.1252	0.1211	0.1196	0.1268	0.1186
χ^2/N_{dof}	0.16	0.47	4.4	4.4	0.84	1.89
ARIADNE	0.1285	0.1268	0.1234	0.1212	0.1258	0.1202
χ^2/N_{dof}	0.96	0.52	2.5	3.1	2.15	1.41
HERWIG	0.1256	0.1242	0.1253	0.1203	0.1258	0.1203
χ^2/N_{dof}	0.5	0.65	4.4	2.0	2.15	0.8
HW++	0.1242	0.1228	0.1299	0.1212	0.1238	0.1168
χ^2/N_{dof}	6.6	3.2	3.3	1.33	2.65	0.56
HW++ MCNLO	0.1234	0.1220	0.1292	0.1220	0.1232	0.1175
χ^2/N_{dof}	10.7	4.2	2.2	1.1	5.7	0.69
HW++ POWHEG	0.1189	0.1179	0.1236	0.1169	0.1224	0.1142
χ^2/N_{dof}	1.46	2.55	3.8	3.9	1.54	0.56

Table 15: Fit results for $\alpha_s(M_Z)$ using LEP1 data and NLL0+NLLA but different hadronisation corrections. In all cases the same detector corrections, obtained from a full detector simulation using PYTHIA as generator is applied. The statistical errors are essentially unaltered compared to those in Table 3.